NAVAL POSTGRADUATE SCHOOL
Monterey, California

THESIS

PROTOTYPE FABRICATION AND MEASUREMENTS OF UPLINK AND DOWNLINK MICROSTRIP PATCH ANTENNAS FOR NPSAT-1

by

İlhan Gökben

March 2003

Thesis Advisor:	Jovan Lebaric
Second Reader:	Richard W. Adler

Approved for public release; distribution is unlimited

THIS PAGE INTENTIONALLY LEFT BLANK

REPORT DOCUMENTATION PAGE			Form Approved OMB No. 0704-0188
Public reporting burden for this collection of information is estimated to average 1 hour per response, including the time for reviewing instruction, searching existing data sources, gathering and maintaining the data needed, and completing and reviewing the collection of information. Send comments regarding this burden estimate or any other aspect of this collection of information, including suggestions for reducing this burden, to Washington headquarters Services, Directorate for Information Operations and Reports, 1215 Jefferson Davis Highway, Suite 1204, Arlington, VA 22202-4302, and to the Office of Management and Budget, Paperwork Reduction Project (0704-0188) Washington DC 20503.			
1. AGENCY USE ONLY ***(Leave blank)***	**2. REPORT DATE** March 2003	**3. REPORT TYPE AND DATES COVERED** Master's Thesis	
4. TITLE AND SUBTITLE: Prototype Fabrication and Measurements of Uplink and Downlink Microstrip Patch antennas for NPSAT-1			**5. FUNDING NUMBERS**
6. AUTHOR(S) **İlhan Gökben**			
7. PERFORMING ORGANIZATION NAME(S) AND ADDRESS(ES) Naval Postgraduate School Monterey, CA 93943-5000			**8. PERFORMING ORGANIZATION REPORT NUMBER**
9. SPONSORING /MONITORING AGENCY NAME(S) AND ADDRESS(ES) N/A			**10. SPONSORING/MONITORING AGENCY REPORT NUMBER**
11. SUPPLEMENTARY NOTES The views expressed in this thesis are those of the author and do not reflect the official policy or position of the Department of Defense or the U.S. Government.			
12a. DISTRIBUTION / AVAILABILITY STATEMENT Approved for public release; distribution is unlimited			**12b. DISTRIBUTION CODE**
13. ABSTRACT (maximum 200 words) This thesis addresses the prototyping, measurement, and validation of two circularly polarized microstrip patch antennas designed by LTJG Mahmut Erel for the NPSAT-1. The antenna system (receive and transmit), consisting of two antennas on a ground plane and their feed systems, was field-tested. The results were compared to the CST® Microwave Studio™ Finite Difference Time Domain (FDTD) software package predictions in order to verify that this design satisfies the NPSAT-1 requirements for bandwidth, free-space radiation pattern and low-profile shape.			
14. SUBJECT TERMS NPSAT-1, NPSAT-1 Antenna System, Microstrip Patch Antenna, Low Power Satellite Antennas, Low Profile Satellite Antennas, Antenna Prototyping, Antenna Measurements, Antenna Design.			**15. NUMBER OF PAGES** 71 **16. PRICE CODE**
17. SECURITY CLASSIFICATION OF REPORT Unclassified	**18. SECURITY CLASSIFICATION OF THIS PAGE** Unclassified	**19. SECURITY CLASSIFICATION OF ABSTRACT** Unclassified	20. LIMITATION OF ABSTRACT Unlimited

NSN 7540-01-280-5500 Standard Form 298 (Rev. 2-89)
Prescribed by ANSI Std. 239-18

THIS PAGE INTENTIONALLY LEFT BLANK

Approved for public release; distribution is unlimited

PROTOTYPE FABRICATION AND MEASUREMENTS OF UPLINK AND DOWNLINK MICROSTRIP PATCH ANTENNAS FOR NPSAT-1

İlhan Gökben
Lieutenant Junior Grade, Turkish Navy
B.S., Turkish Naval Academy, 1996

Submitted in partial fulfillment of the
requirements for the degree of

MASTER OF SCIENCE IN ELECTRICAL ENGINEERING

from the

NAVAL POSTGRADUATE SCHOOL
March 2003

Author: İlhan Gökben

Approved by: Jovan Lebaric
Thesis Advisor

Richard W. Adler
Second Reader and Co-Advisor

John P. Powers
Chairman, Department of Electrical and Computer Engineering

THIS PAGE INTENTIONALLY LEFT BLANK

ABSTRACT

This thesis addresses the prototyping, measurement and validation of two circularly polarized microstrip patch antennas designed by LTJG Mahmut Erel for the NPSAT-1. The antenna system (receive and transmit), consisting of two antennas on a ground plane and their feed systems, was field-tested. The results were compared to the CST® Microwave Studio™ Finite Difference Time Domain (FDTD) software package predictions in order to verify that this design satisfies the NPSAT-1 requirements for bandwidth, free-space radiation pattern and low-profile shape.

THIS PAGE INTENTIONALLY LEFT BLANK

TABLE OF CONTENTS

LIST OF FIGURES

LIST OF TABLES

THIS PAGE INTENTIONALLY LEFT BLANK

ACKNOWLEDGMENTS

Numerous individuals through their advice, encouragement, and technical expertise assisted me in completing this thesis. I am indeed grateful for all their invaluable contributions.

Of those who helped me, a few stand out as having played key roles. Professor Jovan Lebaric provided direction and support in all ways and allowed me to combine my academic experience with a truly challenging and enjoyable project.

Also, Professor Richard W. Adler's technical expertise, relentless support, clear explanations and advice were invaluable.

I would like to thank my friend and my colleague, Mahmut Erel. I could not have finished this thesis without his support, patience and assistance.

I would also like to express my great thanks to David Rigmaiden, who as an engineer always anticipated and resolved any problems I encountered. I greatly appreciate how he always encouraged me throughout this project.

I also want to thank Dan Sakoda along with the entire NPSAT-1 Engineering Staff for their patience, help and contribution.

Finally, I would like to thank my beautiful wife, Sibel Gökben. She was always there to provide me support, encouragement, strength and devotion when I needed it most. I could not have finished without her.

THIS PAGE INTENTIONALLY LEFT BLANK

EXECUTIVE SUMMARY

The purpose of this thesis is to prototype and to validate by measurements, the design of two circularly polarized microstrip patch antennas for the Naval Postgraduate School Spacecraft Architecture and Technology Demonstration Satellite (NPSAT-1). The original design of the antennas was completed by LTJG Mahmut Erel using the CST® Microwave Studio™ Finite Difference Time Domain (FDTD) software package.

As the initial step of this research, the receiving and the transmitting antennas of NPSAT-1 and their feed systems were constructed. To compare the FDTD software results detailed in Ref.1 with measured data, tests were conducted in two parts. In the first part where the antenna system was tested without the NPSAT-1 body model, the results were significantly close to the FDTD software results. Since software predictions were for circular polarization, the test data, which contains only linear polarization, should be approximately 3 dB below predicted values. However, due to frequency limitations of the anechoic chamber, the measured data contained multipath effects, which resulted in increased gain levels, mainly on one side of the antenna beam. The tests showed that the mean values for the 0-dB and the 3-dB beamwidths for the receiving antenna, including two different polarizations, were 93.5˚ and 65.5˚, respectively. For the transmitting antenna these values were 92.8˚ and 70.3˚. The comparison of these values with predictions was made after accounting for multipath effects. Because of the multipath effects (electromagnetic reflections from the interior of the anechoic chamber) and since the differences between measured and estimated gain levels are far more prominent for horizontal polarization (HPOL) than for vertical polarization (VPOL), the values measured for HPOL have not been included in the comparison. Similarly, only the calculated total field magnitude and Left-Hand Circularly Polarized (LHCP) field magnitude values were included, since LHCP is the preferred polarization type for NPSAT-1. The results for the receive antenna show that the mean value for the 0 dB beamwidth was 78.3˚ while the 3--dB beamwidth predicted mean value was 99.3˚. Also, the 3-dB beamwidth value was 52.6˚ for the measured data and 78˚ for the calculated data for the receiving antenna. The

average value of the 0-dB beamwidth for the measured data was 21.1% lower than the predicted value, while the 3-dB beamwidth for the measured data was 32.4% lower than the predicted value. Furthermore, the mean value for the maximum measured gain was 4.72 dB, while the predicted value was 6.93 dB. This shows a 31.8% (2.21 dB) difference between measured and predicted values. For the transmitting antenna, the mean values of the 0-dB beamwidth for the measured and for the computed data were 82.6˚ and 108.3˚ respectively. The difference is 23.7%. For the 3-dB beamwidth these values are 57.6˚ and 88˚ respectively, the difference is 34.4%. In addition, the mean values for the maximum gain were 6.63 dB for the measured data and 8.42 dB for the calculated data, with a difference of 21.2% (1.79 dB). The theoretical difference, for pure LHCP and linear polarization measurements without multipath, should have been exactly 3 dB. Therefore, the peak gain measurements are close (less than 1.21 dB) to the predicted values. In addition to gain measurements, VSWR values were also measured and compared. Measured VSWRs for the prototype antennas are 1.89 for the transmitting antenna and 1.77 for the receiving antenna, compared to computer-predicted values of 2.00 and 1.86, respectively. Hence, 5.56% improvement in the transmitting antenna VSWR and 4.98% improvement in the receiving antenna VSWR were observed. All of these results detailed above verified that Erel's design satisfied the NPSAT-1 requirements.

In the second part of the experiment, the antennas were installed on the NPSAT-1 body model, which was made from wood and heavy aluminum foil. The main effect of the body model was observed on the main lobe and the side lobe gain levels. The main lobes were widened and flattened due to the electromagnetic reflection from the surface of the satellite body. This resulted in at least 2-dB reduction in maximum gain. Similarly, the mean and the standard deviation for the 0-dB beamwidth decreased by 2.5% and 10.9%, respectively. For the 3-dB beamwidth, these values also decreased by 1.65% and 41.4% respectively. In summary, the body model of NPSAT-1 affected the antenna beamwidths favorably by providing more uniform coverage regardless of the satellite orientation.

In conclusion, the field tests and FDTD software models met the NPSAT-1 antenna system design goals. In addition to the pre-launch specification of fitting into the EPAS

canister, the antenna system design satisfies the NPSAT-1 requirements on impedance bandwidth, low profile configuration, and broad coverage radiation pattern. The SWR values are also within the NPSAT-1 requirement of maximum SWR of 2:1. Therefore, this design can be accepted as the NPSAT-1's antenna system.

THIS PAGE INTENTIONALLY LEFT BLANK

I. INTRODUCTION

A. OBJECTIVES

The objective of this thesis is to validate the antenna design for the Naval Postgraduate School Spacecraft Architecture and Technology Demonstration Satellite (NPSAT-1) antenna system. LTJG Mahmut Erel was responsible for the original antenna design and employed the CST® Microwave Studio™ Finite Difference Time Domain (FDTD) software package to model the NPSAT-1 antenna system. [1]

This thesis completes the NPSAT-1 antenna design effort with the actual antenna construction and measurements. In addition to the FDTD software package, individual antenna prototypes and a 1:1 scale model of the NPSAT-1 satellite were used. In order to achieve more accurate and reliable results, the horn antennas that will be installed in the NPSAT-1 Ground Control Station were also used during the tests.

The measurements include antenna radiation patterns, input impedance and polarization. The radiation pattern data and associated power gains will be used by the Ground Control Station in controlling NPSAT-1's attitude and data transfer during orbit.

B. BACKGROUND

1. The NPSAT-1 Project

NPSAT-1 will be a small, economical and lightweight technology demonstration research satellite. Its primary mission is to conduct a number of experiments for the Naval Research Laboratory (NRL) and the Naval Postgraduate School (NPS). Two of these experiments will include NRL payloads, the coherent electromagnetic radio tomography (CERTO) and a Langmuir probe. The CERTO experiment is used to measure the total electron content (TEC) in the ionosphere. The Langmuir probe will augment CERTO data by providing in-orbit measurements. The information collected will assist in designing the U.S. Navy's next generation communication satellites. The other experiments are of NPS origin. These include a novel design for (1) a spacecraft computer board and (2) a commercial, off-the-shelf (COTS) visual imager (VISIM) which is a

digital camera, a configurable processor experiment (CPE), solar cell measurement system (SMS) and a three-axis micro-electromechanical systems (MEMS)-based rate gyro.

NPSAT-1's primary mission is also to expose NPS students to the full life-cycle development of a space system. Some of the primary objectives of this project are as follows:

- To provide spacecraft development on a low budget
- To give officer students experience in its design, development, integration, and testing
- To provide students with in-orbit operations and flight operations experience while at NPS.

NPSAT-1 will demonstrate COTS technology in spacecraft architecture as a means of decreasing development time and increasing reliability in software development. It will also provide a space platform for future scientific experiments. In addition, NPSAT-1 will also demonstrate new technologies, such as nonvolatile ferroelectric RAM (which is inherently radiation tolerant), advanced triple-junction (ATJ) solar cells, SONY® US18650S Lithium-ion batteries and a COTS-based, Personal Computer (PC) compatible command and data handling subsystem.

A group of full-time engineers, employed by the Space System Academic Group (SSAG) at NPS, supports this innovative and challenging project. Many NPS thesis students, who will continue to participate in this effort, will be assisting these engineers when NPSAT-1 nears its final preparations and tests for the earliest launch in March 2006. Figure 1 illustrates the NPSAT-1 with its antennas.

2. Spacecraft Description

The satellite weighs 180 pounds, and is a 12-sided cylindrical polygon that is approximately 34 inches long and 20 inches in diameter. As a part of the Department of Defense (DOD) Space Test Program (STP) MLV-05 Delta IV mission, NPSAT-1 will be jettisoned via an Evolved Expendable Launch Vehicle (EELV), using an EELV Secondary Payload Adapter (ESPA) canister. Then the satellite will be inserted into a circular Low Earth Orbit (LEO) of 560 km ± 10 km altitude with 35.4^{o} inclination.

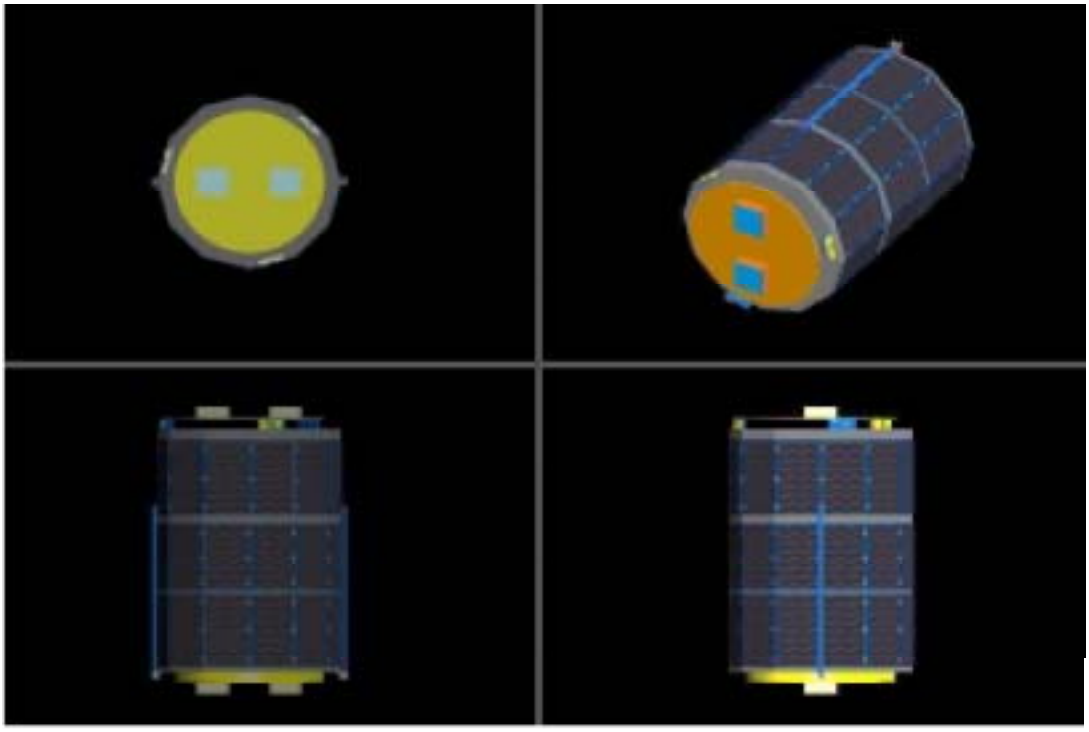

Figure 1. NPSAT-1 with Antennas

NPSAT-1 is being constructed of a robust 6061-T6 aluminum frame and panels and will be anodized and thermally protected after integration at the flight site. Triple junction solar cells, which are calculated to have at least 24% efficiency, will be attached to the sides of the spacecraft to power the satellite as it tumbles in orbit. The top and bottom of the spacecraft will not have solar cells attached to them, since the antennas will be placed there.

NPSAT-1 will have a full-duplex Gaussian-filtered Minimum Shift Keying (GMSK) communication system. GMSK modulation has been chosen because of its excellent power and spectral efficiencies. Even though the pre-modulation of the Gaussian-filtering introduces inter-signal interference (ISI) in the transmitted signal, the degradation is not severe if the 3-dB bandwidth-bit duration product of the filter is greater than 0.5. GMSK sacrifices the irreducible error rate caused by partial response signaling in exchange for extremely good spectral efficiency and constant envelope properties [2]. The transmit frequency and the receive frequency for this communication system are 2207.3 MHz and 1767.565 MHz, respectively. The satellite will be able to store up to 256

MB of memory, and to send and receive messages at the rate of 100 kilobits per second as it passes overhead. Figure 2 shows an expanded view of NPSAT-1 and its subsystems.

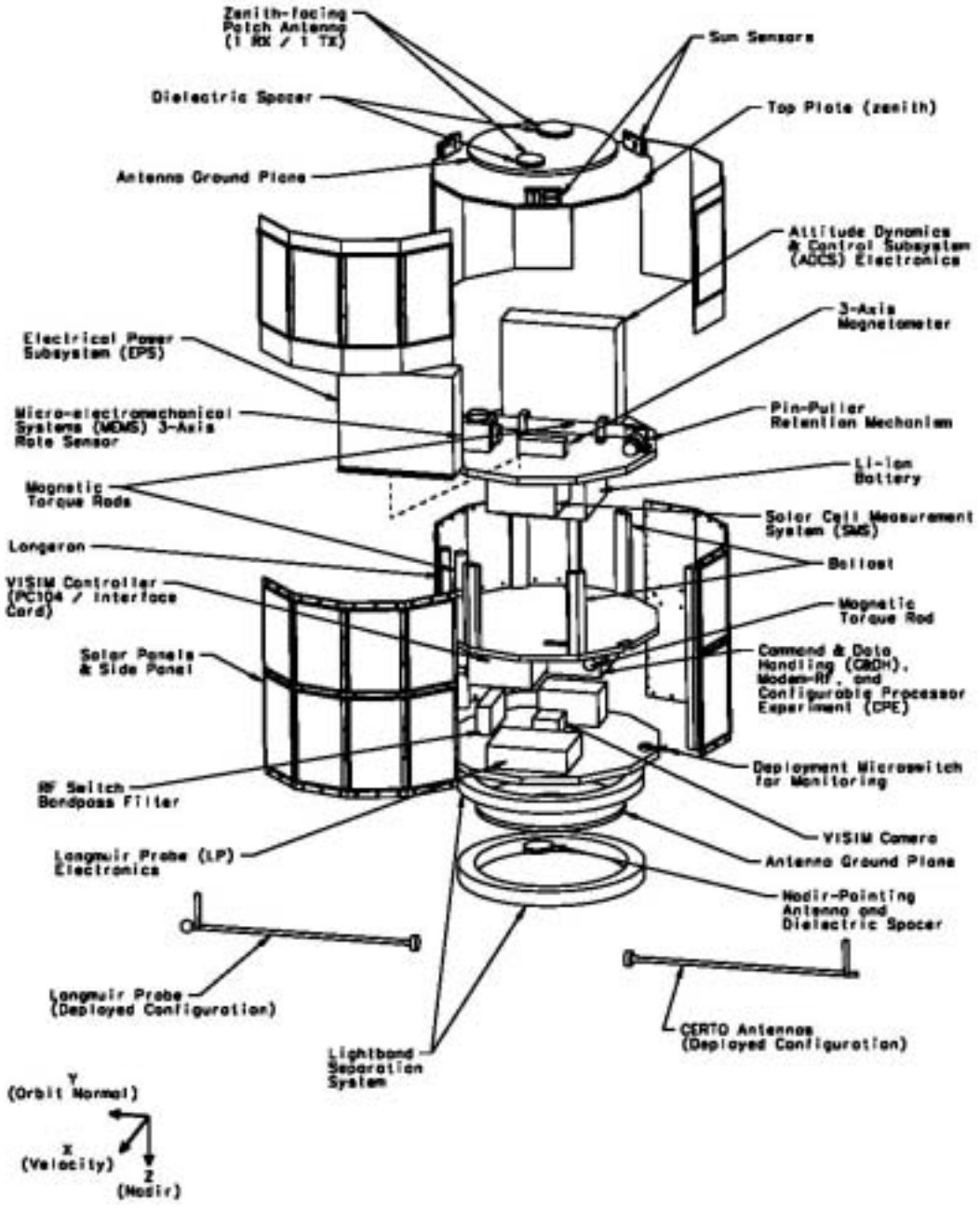

Figure 2. Expanded View of NPSAT-1 and Its Subsystems [from NPSAT-1 Team]

C. TESTING METHODOLOGY

The initial step of this research consisted of constructing the antennas and feed system designed by LTJG Mahmut Erel. Details of this design and specifications for the antennas can be found in Chapter II.

After the antennas and the feed system were constructed, they were integrated onto a 1:1 scale model of NPSAT-1, made from wood and heavy aluminum foil. This model was then field-tested. The primary goal was to match the antenna impedances to 50 Ω with a Standing Wave Ratio (SWR) of less than or equal to 2:1. This process is described in detail in Chapter III.

Once the prototyping and testing were completed, the data was compared to the FDTD software package results in order to verify that this design satisfied the NPSAT-1 requirements for bandwidth, free-space radiation pattern and low-profile shape. These comparisons are detailed in Chapter IV.

THIS PAGE INTENTIONALLY LEFT BLANK

II. DESIGN DETAILS AND ANTENNA SPECIFICATIONS

In this chapter, the computer-based design of the NPSAT-1 antennas is described in detail. This includes the design specifications based upon the NPSAT-1 system requirements, the resulting antenna design concept and dimensions, as well as a brief introduction to the prototyping phase.

A. DESIGN DETAILS

The design of the antenna elements was constrained by the following requirements:

- The NPSAT-1 must fit into an Evolved Secondary Payload Adapter (ESPA) canister, unimpeded by antennas
- Due to the constant motion of the satellite and the Ground Control Station's linearly polarized antennas, NPSAT-1 antennas must provide circular polarization
- Antenna assembly must be light and simple for repeated construction
- Antennas must have a radiation pattern wide enough to prevent coverage loss if the satellite loses its directional capability
- The antennas should not dissipate any power, that is, the antennas should radiate efficiently.

In order to satisfy these requirements, the design depicted in Figure 3 was chosen.

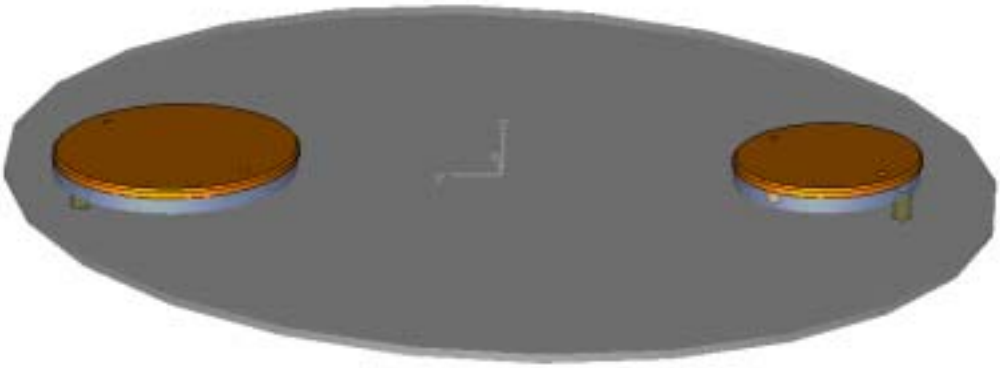

(a) The Receiving (left) and the Transmitting Antenna (right) for the Top Side of the Satellite

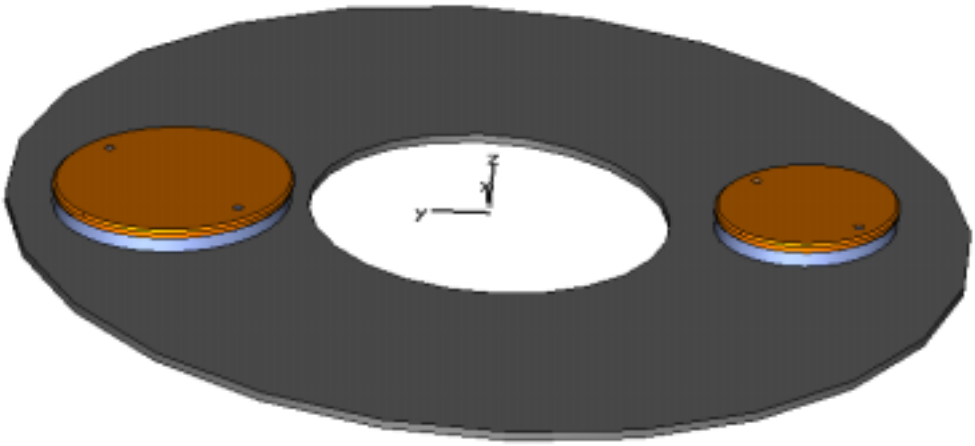

(b) The Receiving (left) and the Transmitting Antenna (right) for the Bottom Side of the Satellite

Figure 3. NPSAT-1 Antenna System [from Ref.1]

The antenna elements, once integrated onto NPSAT-1, must fit within the EPAS canister. The clearance between the spacecraft and the interior sides of the canister is approximately two inches. Therefore, a flat antenna design is necessary.

Because of the mechanical restrictions, a patch antenna design was preferred to meet the requirements for polarization, efficiency and radiation pattern. As illustrated in Figure 3, this configuration consisted of a ground plane and two relatively small metal plates, called patches, which will function as uplink and downlink antennas. A circular ground plane was the choice to best fit on the top and the bottom of the satellite. The greatest challenge was to determine the actual shape and dimensions of the patches.

From the circularly polarized patch designs detailed in Ref. 3, an elliptical shaped patch antenna was chosen. These copper elliptical patches (one is the transmitter and the other is the receiver) were placed on an aluminum ground plane with optimum surface area, while providing maximum clearance from each other and from the edges of the ground plane. This was accomplished by rotating the antennas 45^{o} counterclockwise around their respective centers. The actual antennas on the aluminum ground plane mounted on the NPSAT-1 model are shown in Figure 4.

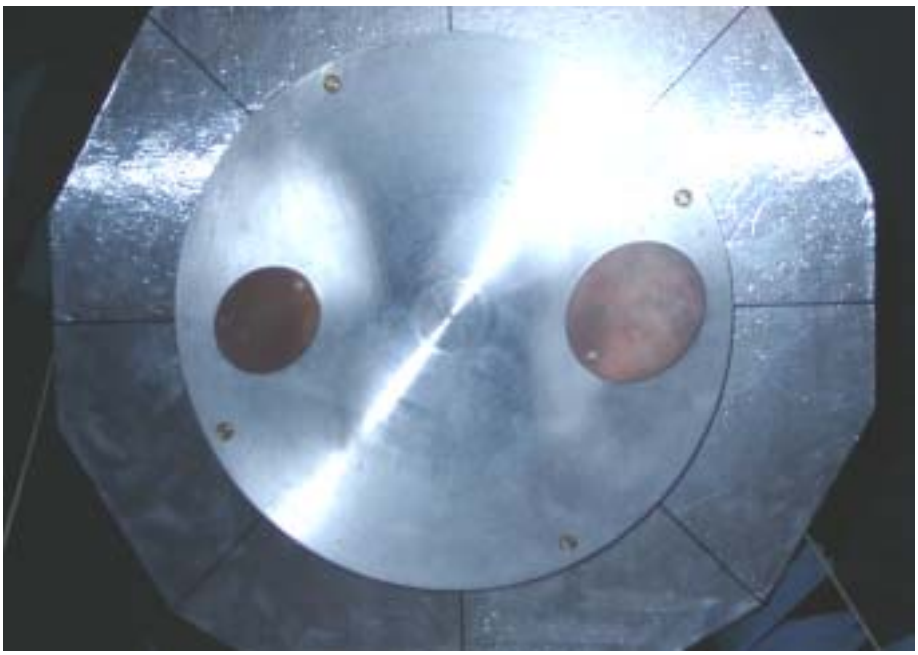

Figure 4. Patch Antennas and Ground Plane

Coaxial cables provided the feeds for both antennas. These cables were first attached to the bottom of the ground plane with SMA connectors. The positions of the feeds relative to the patch centers were carefully chosen to simultaneously achieve good impedance match and circular polarization. Hence, they were placed 45^{o} diagonally from

the main axes of the ellipses. A Teflon dielectric substrate was inserted between the patches and the ground plane to provide patch support and to increase the mechanical strength. One metal screw ("post") per patch was used to improve the impedance bandwidth and to maintain mechanical rigidity of the antennas, and was placed opposite to the feed points. Figure 5 shows a detailed picture of the feed connection.

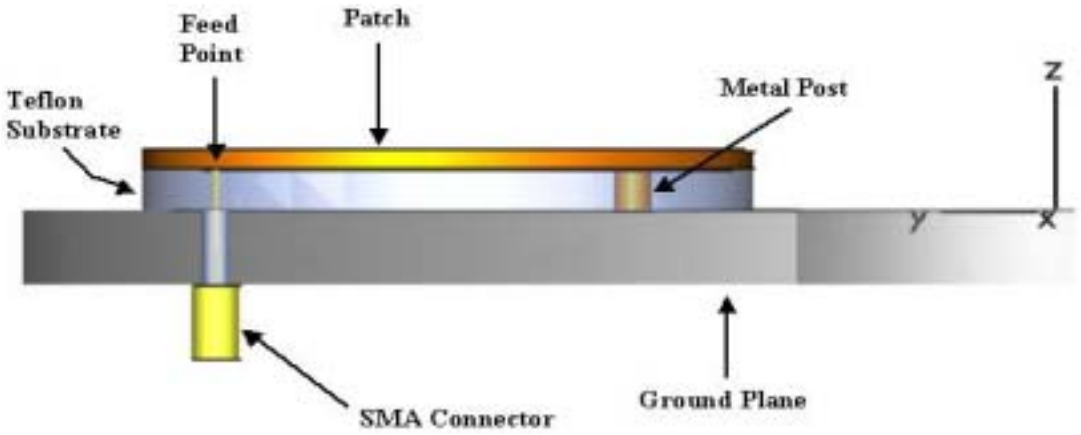

Figure 5. Feed System and SMA Connection

Another important issue regarding the antenna design was obtaining a radiation pattern that provides adequate coverage towards the earth. That is, the spacecraft must receive and transmit signals at any given time, for a wide range of satellite orientations. This was accomplished by using microstrip patch antennas that have nearly hemispherical radiation patterns. In the nominal case, where the Attitude Control Subsystem (ACS) maintains the satellite in the nadir-pointing direction properly, only the nadir-pointing (bottom) antennas will be used. Figure 6 illustrates the NPSAT-1's predicted attitude.

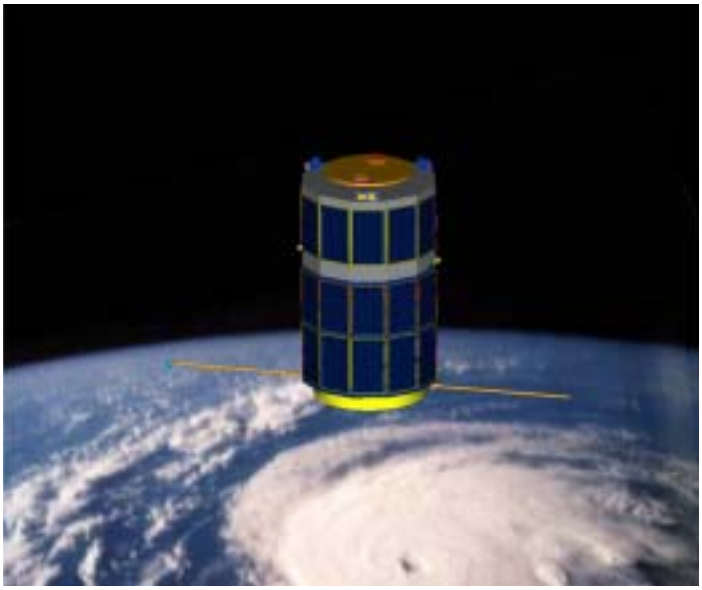

Figure 6. NPSAT-1's Predicted Attitude.

However, in the event that the satellite loses its pointing capability, the antenna system must function in either the nadir-pointing direction or in the zenith-pointing direction. To ensure that this criterion is met, two separate antenna groups based on the same design will be installed on the satellite. Because the VISIM digital camera will be placed on the bottom of the satellite, the bottom antenna group was designed to have a different ground plane, with a four-inch hole in the center.

B. ANTENNA SPECIFICATIONS AND DIMENSIONS

After numerous trials to meet all the mechanical and electrical requirements, the dimensions in the following tables were designated as final design parameters.

CYLINDRICAL ALUMINUM GROUND PLANE (for both antennas)			
Diameter	32 cm		
Hole diameter (for the bottom antenna)	12 cm		
Thickness	0.636 cm		
ELLIPTICAL PATCH ANTENNA			
Short Axis (along X-direction)	7.293 cm		
Long Axis (along Y-direction)	8.509 cm		
Thickness	0.318 cm		
DIELECTRIC TEFLON SUBSTRATE			
Short Axis (along X-direction)	7.293 cm		
Long Axis (along Y-direction)	8.509 cm		
Thickness	0.6 cm		
CYLINDRICAL COPPER POST			
Diameter	0.5 cm		
Height	0.7 cm		
COAXIAL CABLE (50 OHMS)			
	Outer Radius	Inner Radius	Height
Coax Center (PEC)	0.056 cm	-	1.868 cm
Coax Dielectric (Teflon)	0.184 cm	0.056 cm	1.318 cm
Coax Shield (PEC)	0.313 cm	0.184 cm	1 cm
TEFLON MOUNTING SCREW			
Diameter	0.15 cm		

Table 1. The NPSAT-1 Receiving Antenna Dimensions.

CYLINDRICAL ALUMINUM GROUND PLANE (for both antennas)			
Diameter	32 cm		
Hole diameter (for the bottom antenna)	12 cm		
Thickness	0.636 cm		
ELLIPTICAL PATCH ANTENNA			
Short Axis (along X-direction)	5.66 cm		
Long Axis (along Y-direction)	6.6 cm		
Thickness	0.318 cm		
DIELECTRIC TEFLON SUBSTRATE			
Short Axis (along X-direction)	5.66 cm		
Long Axis (along Y-direction)	6.6 cm		
Thickness	0.6 cm		
CYLINDRICAL COPPER POST			
Diameter	0.5 cm		
Height	0.7 cm		
COAXIAL CABLE (50 OHMS)			
	Outer Radius	Inner Radius	Height
Coax Center (PEC)	0.056 cm	0 cm	1.868 cm
Coax Dielectric (Teflon)	0.184 cm	0.056 cm	1.318 cm
Coax Shield (PEC)	0.313 cm	0.184 cm	1 cm
TEFLON MOUNTING SCREW			
Diameter	0.15 cm		

Table 2. The NPSAT-1 Transmitting Antenna Dimensions.

C. PROTOTYPING

In his thesis, LTJG Mahmut Erel verified the final designs for the two antennas by using the FDTD software package. According to Ref.1, all parameters met the prerequisites of the NPSAT-1 antenna system. However, the antenna designs had to be validated by measurements. Therefore, all the antenna elements described in this chapter were

constructed, integrated and attached to the NPSAT-1 body model. The testing method and the results are discussed in Chapter III.

This chapter has detailed the dimensions of NPSAT-1's antennas and the impact of the satellite's physical constraints on the design details.

III. PROTOTYPE MEASUREMENTS

In this chapter, the testing methodology and results of tests for the two antenna prototypes are detailed. Tests were conducted using the top antenna configuration shown in Figure 3a. Because the added mechanical strength was not needed for the tests, the plastic screw holes on the patches were not implemented.

A. SWR MEASUREMENTS OF THE ANTENNA PROTOTYPES

The SWR, also known as VSWR, is a mathematical expression of the non-uniformity of electromagnetic field intensity on a transmission line such as coaxial cable. Usually, SWR is defined as the ratio of the maximum radio-frequency (RF) voltage to the minimum RF voltage along the line. The SWR can also be defined as the ratio of the maximum RF current to the minimum RF current on the line [4]. The SWR indicates how much of the electromagnetic energy is transferred to the load and how much is reflected from the end of the transmission line. The SWR is calculated as

$$SWR = \frac{1 - |\Gamma|}{1 + |\Gamma|}, \tag{3.1}$$

$$\Gamma = \frac{Z_{in} - Z_o}{Z_{in} + Z_o}, \tag{3.2}$$

where Γ is the reflection coefficient, Z_o is the characteristic impedance of the line connected to the load input, and Z_{in} is the input impedance of the load.

In the ideal case, in which the load and the line impedances are identical, the SWR is equal to 1. However, since the antenna input impedance in general has a reactive component and the real part of the antenna input impedance varies with frequency, the SWR is, in practice, always greater than 1. For NPSAT-1, the SWR requirement is a maximum value of 2:1.

The SWR measurements of the prototype antennas were performed using the Hewlett-Packard® (HP) 8510C Network Analyzer and the HP 8517A S-parameter Test

Set. The Network Analyzer was used to measure the reflection coefficient and to calculate the SWR of the antennas while the S-parameter Test Set simulated the calibrated transmission line. For the transmitting antenna, operating at 2207.3 MHz, the SWR from S-parameter measurements was 1.89, and for the receiving antenna, the SWR was 1.77. Since the required 300 kHz bandwidths for the two antennas are narrow relative to the center frequency, the S-parameter values measured over the required bandwidth were essentially constant and the SWRs were effectively equal to the above values. Both antenna prototypes satisfied the NPSAT-1 SWR requirement of 2:1 or lower over their operating frequency ranges.

B. RADIATION PATTERN MEASUREMENTS

All tests detailed here were performed in three major steps, as outlined below.

1. The Antenna-Under-Test (AUT) and Anechoic Chamber Calibrations

The anechoic chamber is a specifically designed and constructed facility for antenna measurements and electromagnetic interference (EMI) testing. The walls of the interior chamber are fabricated from special conducting wallboard with an overlay of microwave frequency absorber (blue foam). Figure 7 illustrates the interior of the NPS anechoic chamber.

The anechoic chamber test facility consists of the following equipment:

- HP® 8510C Network Analyzer (45 MHz to 50 GHz)
- HP® 8511A Frequency Converter (45 MHz to 26.5 GHz)
- HP® 8348A Microwave Amplifier (+20 dBm RF max. at 2 GHz to 26.5 GHz)
- HP® 83631A Synthesized Sweeper (45 MHz to 26.5 GHz)
- National Instruments® Lab VIEW™ 5.1a Software

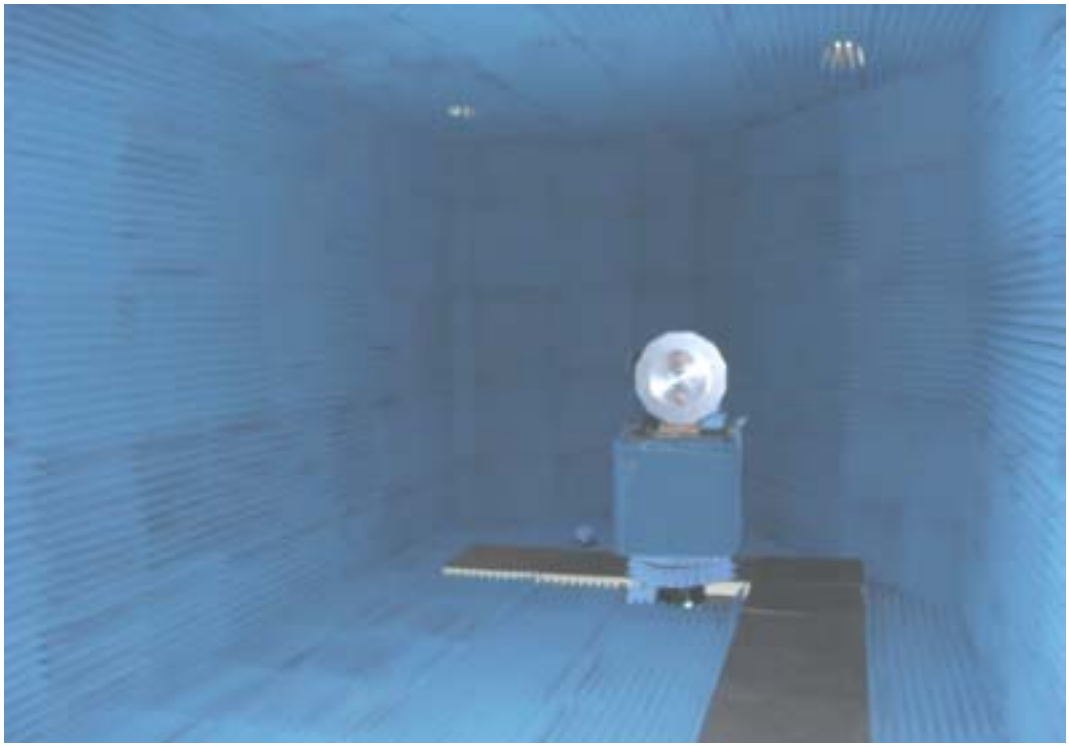

Figure 7. Interior of the Anechoic Chamber.

Anechoic chamber measurements require a calibration to determine the gain levels measured by the Network Analyzer. This was accomplished by using two perfectly matched, equal gain standard horn antennas. One of the antennas was placed into position to illuminate the other horn antenna. A complete test was performed and the maximum signal at the receive antenna was measured as –4 dB, a relative system signal. This value represented the receive and the transmit antennas' nominal maximum gains of 10 dB. Hence, a difference of 14 dB was added to all measured values for the patch antennas. The measured pattern of the 10-dB standard gain antenna is depicted in Figure 8.

After the antenna-under-test (AUT) was calibrated, a wooden support for the antennas was constructed so that the center of the ground plane and the center of the horn antenna were on the same line, within one-inch, and approximately 20 feet (6.1 m) apart from each other. This distance satisfied the minimum far field requirement of 3.652 m. This calculation was made by using the far field distance formula:

$$\text{Far Field Distance} \geq \frac{2 \times D^2}{\lambda}, \tag{3.3}$$

where D is the largest dimension of the source and λ is the operating wavelength. Hence, the minimum far field distance was found as

$$\text{Far Field Distance } \geq \frac{2\times(0.4984)^2}{0.136} = 3.652 \text{ m.}$$

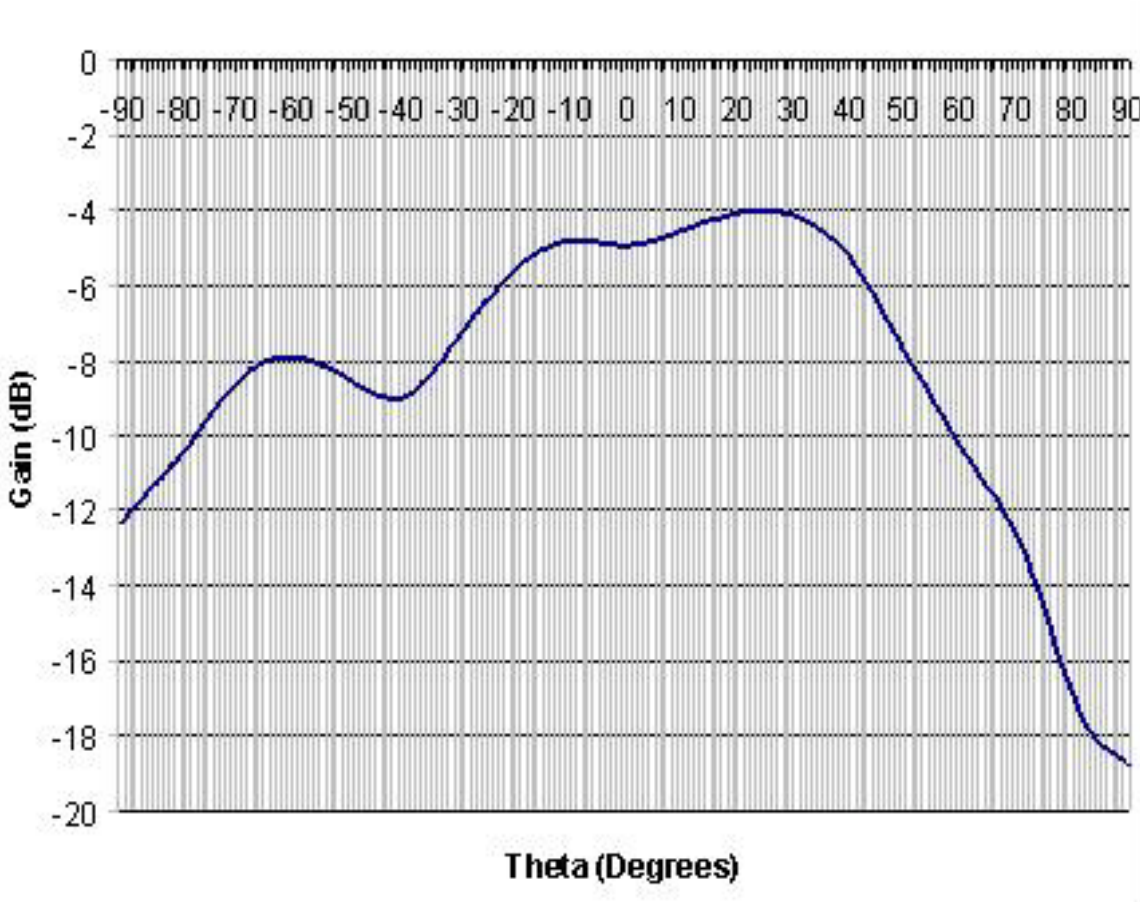

Figure 8. The Measured Radiation Pattern of the 10-dB Standard Gain Horn Antenna.

Additional calculations were performed to ensure that the measured antennas remained within the 1-dB beamwidth of the illuminating horn antenna, while rotating through the θ angle. From Fig. 8, the 1-dB beamwidth was determined to be approximately 39˚. At a distance of 6.1 m where the prototype antennas were placed, this beam was 4.4 m wide, so the rotating receiving antenna was always within the 1-dB beamwidth of the illuminating horn antenna.

Another issue was the polarization of the antennas. Since patterns generated by the satellite antennas have both vertically and horizontally polarized components (VPOL and HPOL), each component was observed separately for each antenna. This was accomplished by rotating the horn antenna axis by 90˚.

2. Measurements without the NPSAT-1 Body Model

This set of measurements compared measured patterns with those from the FDTD software results of Ref. 1, using a reference coordinate system shown in Figure 9.

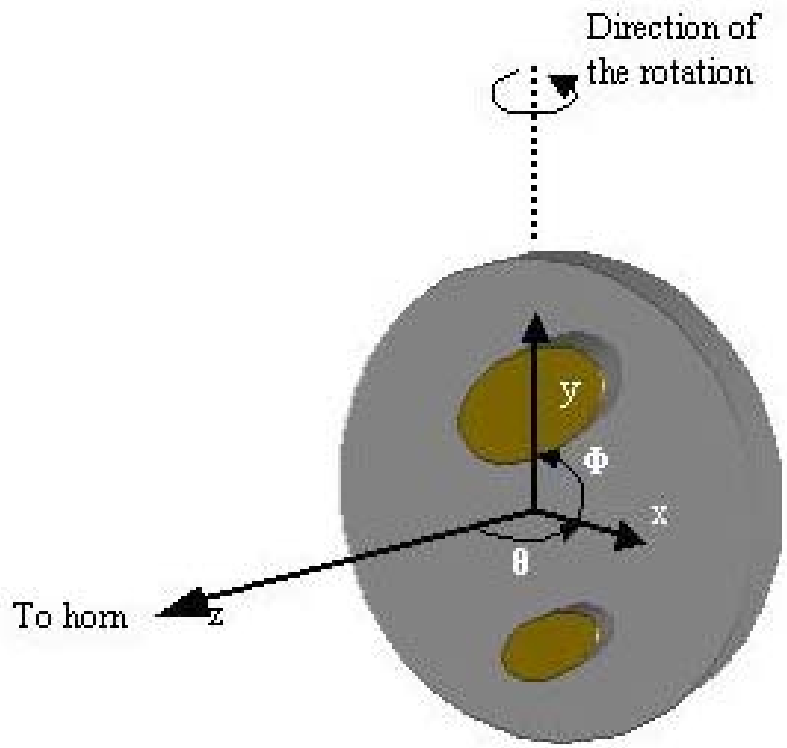

Figure 9. Reference Coordinate System for Prototype Measurements.

a. Test Results for the Receiving and Transmitting Antennas with the Horn Antenna Vertically Polarized (VPOL)

(1) The Antennas Aligned along the Y-axis. The receiving and the transmitting antenna alignments during these tests are depicted in Figure 10. Note that two variations of antenna placement (the transmitting antenna in the upper position, the receiving antenna in the lower position, and vice versa) were tested.

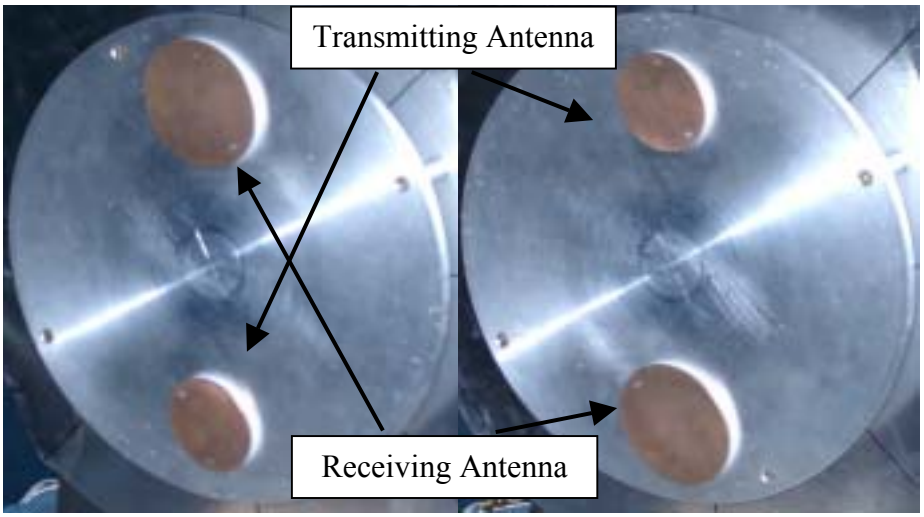

Figure 10. Antenna Test Alignments for the Receiving Antenna ($\Phi = 90^{\circ}$) and the Transmitting Antenna ($\Phi = -90^{\circ}$)

Figure 11 shows the polar plots of the radiation patterns, with the gain in dB relative to an isotropic radiator, for the vertical polarization, in free-space. The polar plots, with the angle measured from the z-axis (the axis normal to the patch antenna surface, see Figure 9), show that the radiation is focused in the desired half-space, away from the satellite, and that transmit and the receive antennas have comparable performance.

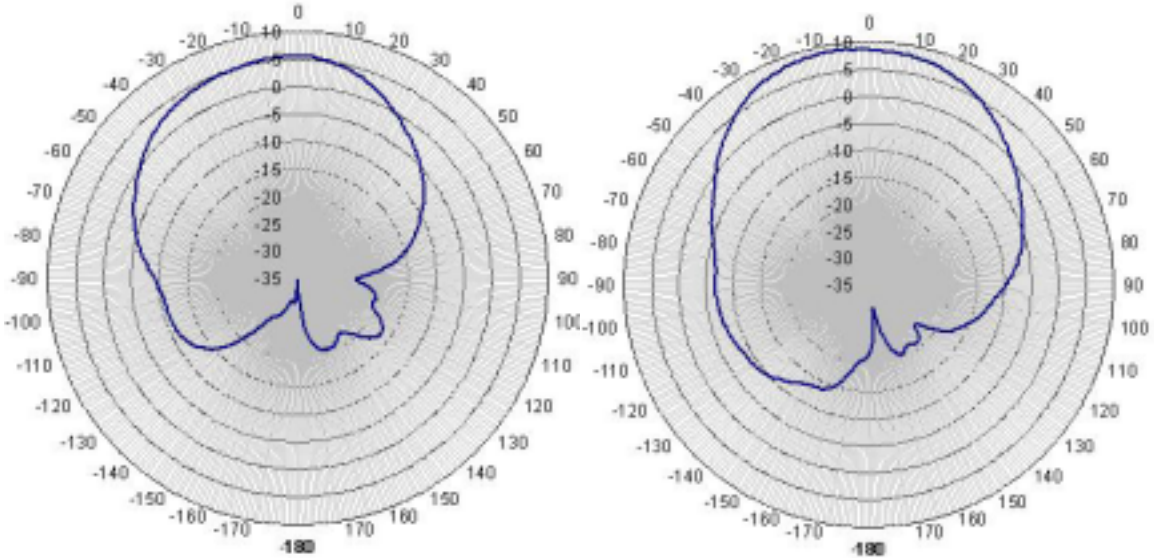

Figure 11. The VPOL Free-space Radiation Patterns of the Receiving Antenna ($\Phi = 90^\circ$) and the Transmitting Antenna ($\Phi = -90^\circ$)

(2) The Antennas Aligned along the X-Axis. The receiving and the transmitting antenna alignments during these tests are illustrated in Figure 12. This was the second alignment tested during the experiments. In this alignment, the receiving antenna is aligned at $\Phi = 0^\circ$ and the transmitting antenna is at $\Phi = 180^\circ$.

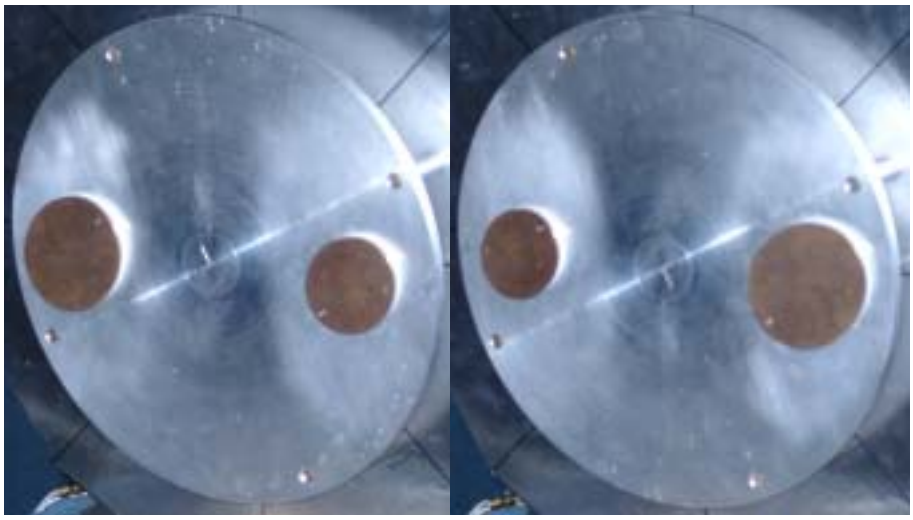

Figure 12. Antenna Test Alignments for the Receiving Antenna ($\Phi = 0^\circ$) and the Transmitting Antenna ($\Phi = 180^\circ$)

Figure 13 shows the radiation patterns, with the gain in dB relative to an isotropic radiator, for the vertical polarization, in free-space, with the alignment shown in Figure 12. The polar plots in Figure 13 show that the radiation is focused in the desired half-space, away from the satellite, and that transmit and receive antennas have comparable radiation patterns, consistent with previously tested alignments.

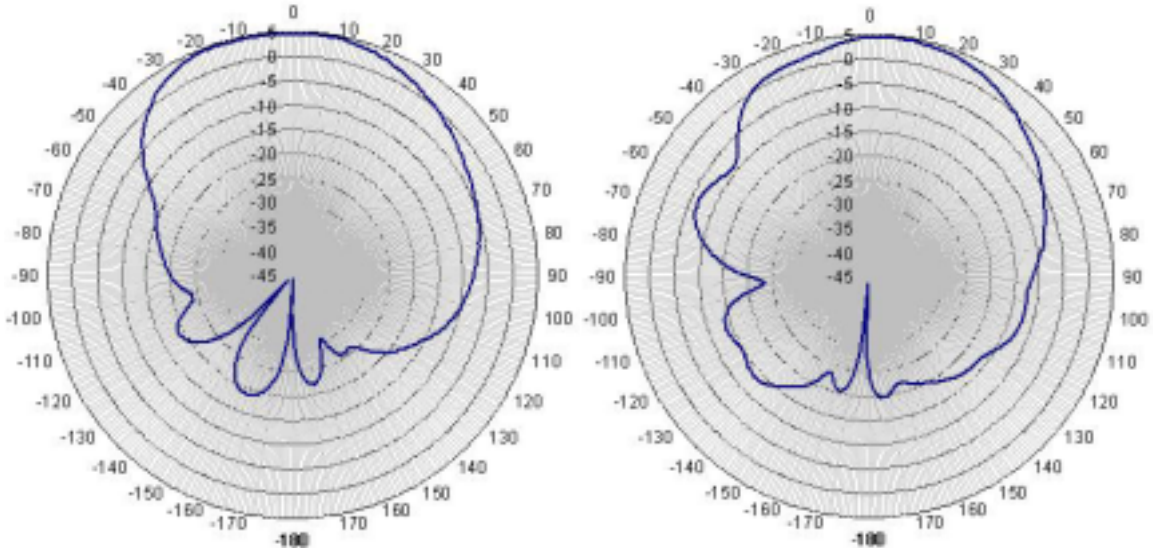

Figure 13. The VPOL Free-space Radiation Patterns for the Receiving Antenna ($\Phi = 0^{\circ}$) and the Transmitting Antenna ($\Phi = 180^{\circ}$)

(3) The Antennas Aligned with a Left 45˚ Offset. Figure 14 illustrates the receiving and the transmitting antenna alignment during these tests. This was the third alignment tested during the experiments. In this alignment, the receiving antenna is aligned at $\Phi = 135^{\circ}$ and the transmitting antenna is at $\Phi = -45^{\circ}$.

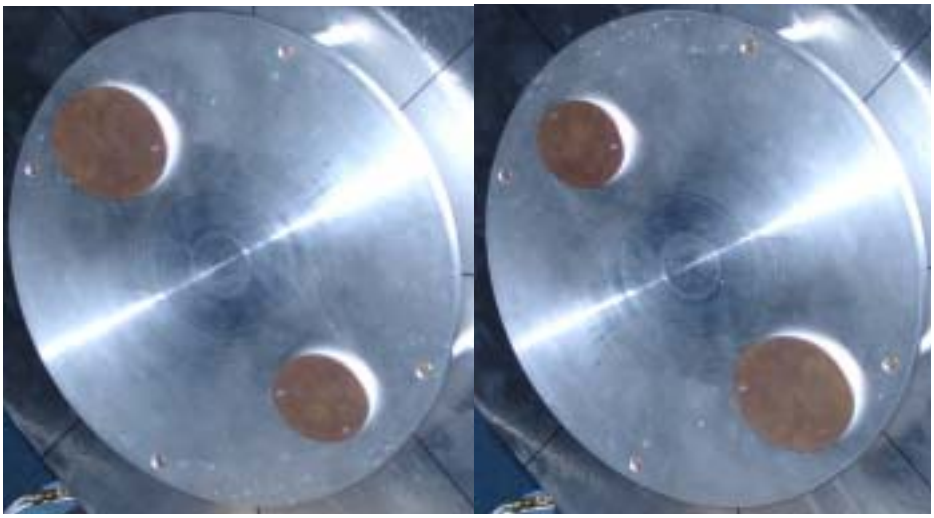

Figure 14. Antenna Test Alignments for the Receiving Antenna ($\Phi = 135^{\circ}$) and the Transmitting Antenna ($\Phi = -45^{\circ}$)

Figure 15 shows the radiation patterns, with the gain in dB relative to an isotropic radiator, for vertical polarization, in free-space, with the alignment shown in Figure 14. The polar plots in Figure 15 show that the radiation is focused in the desired half-space, away from the satellite, and that transmit and receive antennas have comparable radiation patterns. The performance of the antennas remains consistent as alignment changes.

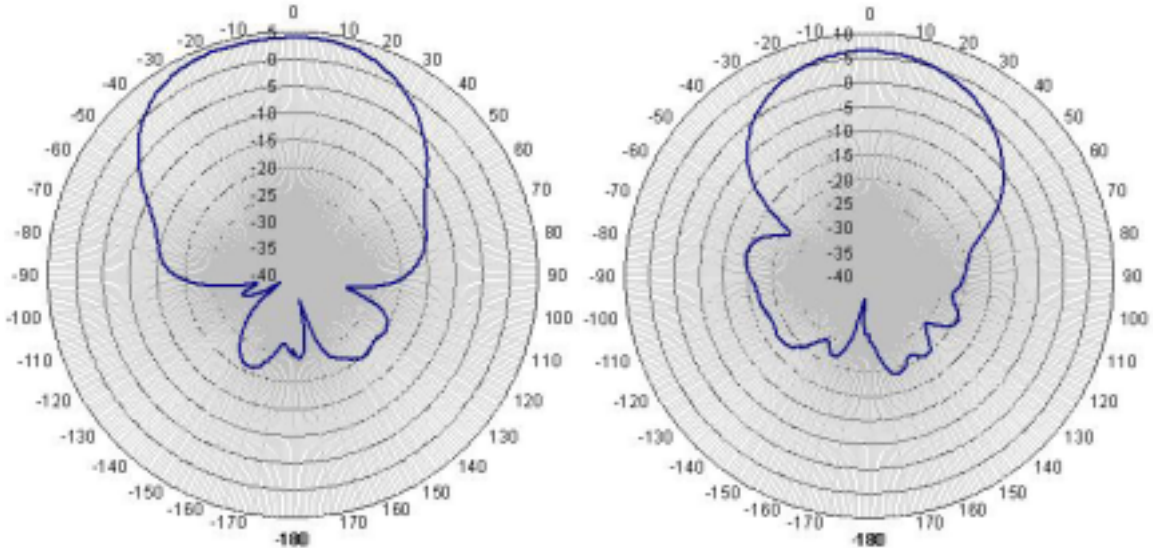

Figure 15. The VPOL Free-space Radiation Patterns of the Receiving Antenna ($\Phi = 135^{\circ}$) and the Transmitting Antenna ($\Phi = -45^{\circ}$)

b. Test Results for the Receiving and Transmitting Antennas with the Horn Antenna Horizontally Polarized (HPOL)

(1) The Antennas Aligned Along the Y-axis. The receiving and the transmitting antenna alignment during these tests are depicted in Figure 10. Figure 16 below shows the resulting horizontally polarized free-space radiation patterns at that alignment. Despite the change from vertical to horizontal polarization, the patterns remain consistent with the patterns observed for the vertical polarization, with radiation focused in the desired half-space (away from the satellite) for both antennas. The pattern consistency with polarization rotation is highly desirable for this application, because of the possible satellite attitude change relative to the ground station antennas.

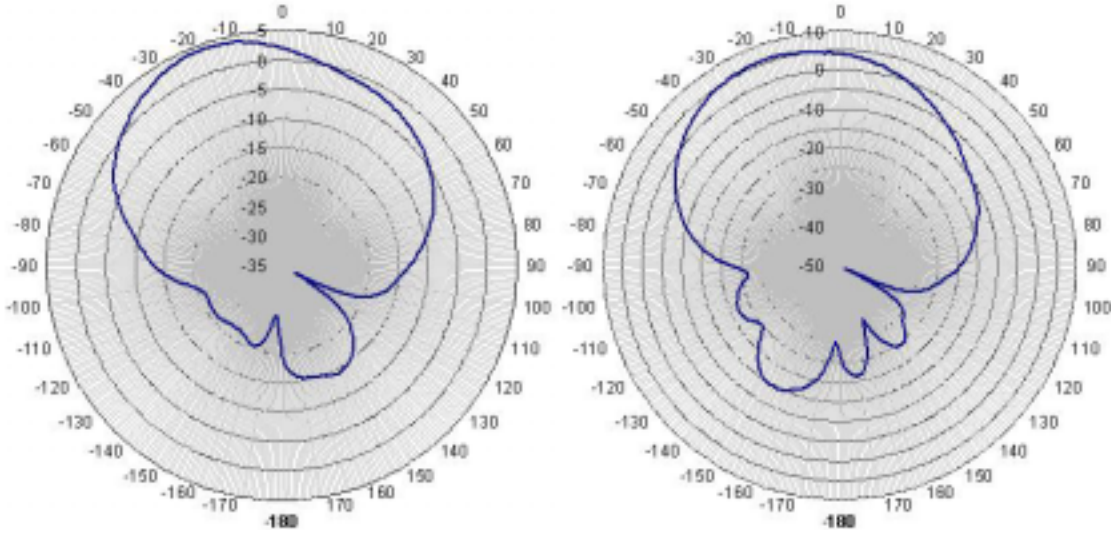

Figure 16. The HPOL Free-space Radiation Patterns of the Receiving Antenna ($\Phi = 90^{\circ}$) and the Transmitting Antenna ($\Phi = -90^{\circ}$)

(2) The Antennas Aligned Along the X-Axis. The receiving and the transmitting antenna alignment during these tests are illustrated in Figure 12. Figure 17 below shows the resulting horizontally polarized free-space radiation patterns at that alignment. The patterns remain consistent with the patterns for the vertical polarization, with radiation focused in the desired half-space (away from the satellite) for both antennas, and with the horizontal polarization patterns for the other alignments.

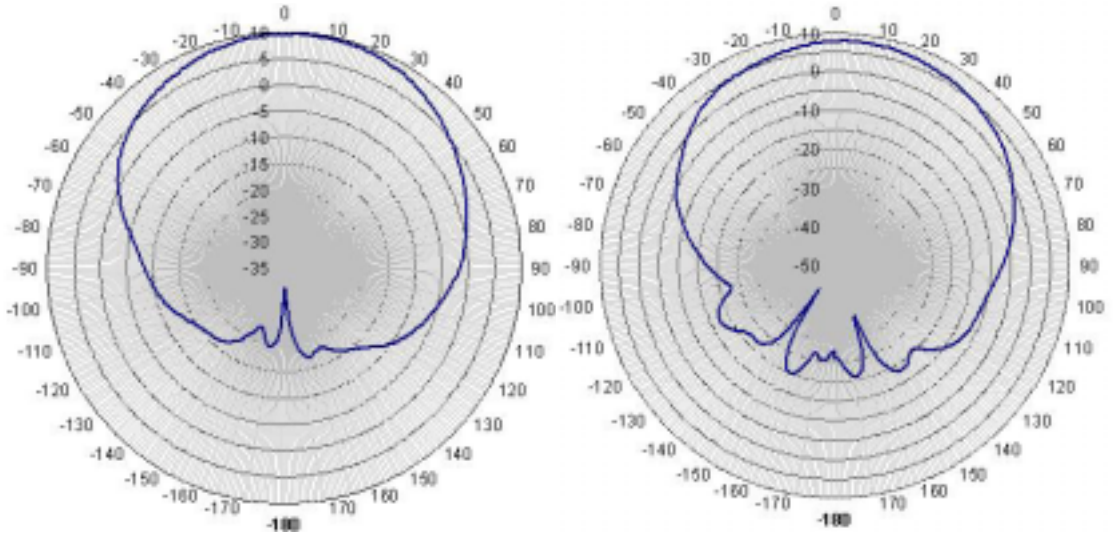

Figure 17. The HPOL Free-space Radiation Patterns of the Receiving Antenna ($\Phi = 0^{\circ}$) and the Transmitting Antenna ($\Phi = 180^{\circ}$)

(3) The Antennas Aligned with a Left 45˚ Offset. The receiving and the transmitting antenna alignment during these tests are illustrated in Figure 14. Figure 18 below shows the resulting horizontally polarized free-space radiation patterns at that alignment. The horizontal polarization patterns are consistent with the vertical polarization patterns, with radiation focused in the desired half-space (away from the satellite) for both antennas, and with the horizontal polarization patterns for the other alignments.

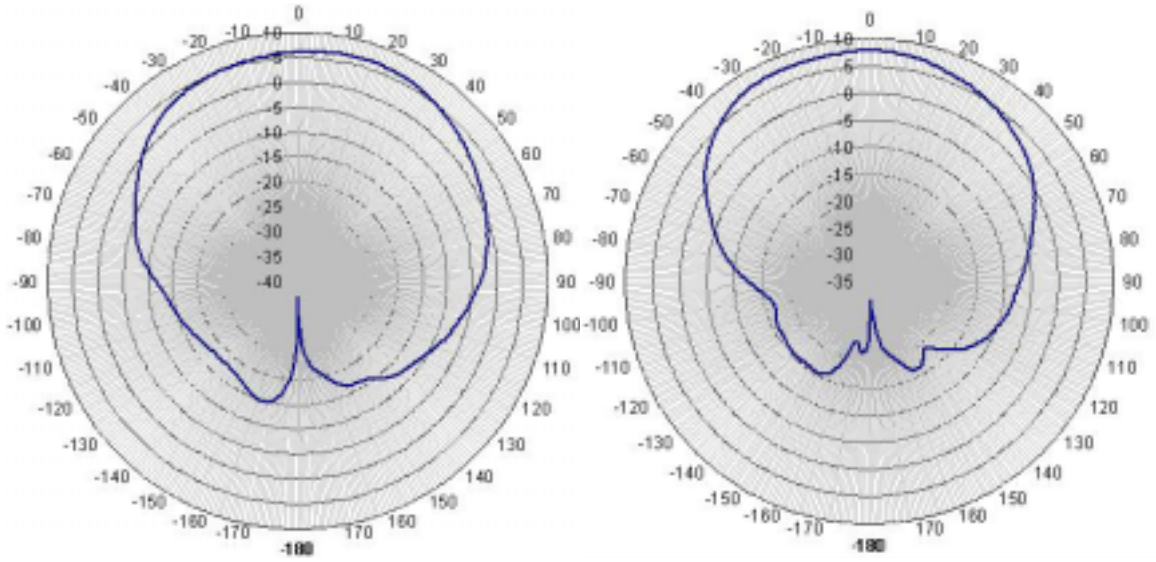

Figure 18. The HPOL Free-space Radiation Patterns of the Receiving Antenna (Φ =135˚) and the Transmitting Antenna (Φ = –45˚)

3. Measurements with the NPSAT-1 Body Model

In this phase of the tests, the antennas and the feed system were integrated onto a 1:1 scale model of NPSAT-1, made from wood and heavy aluminum foil. The purpose of these tests was to observe the effects of NPSAT-1 on the antenna system. Since the satellite will be constructed of a conducting material, total current distribution over the surface of the antennas may be affected.

a. Test Results for the Receiving and Transmitting Antennas on NPSAT-1 with the Horn Antenna Vertically Polarized (VPOL)

(1) The Antennas Aligned Along the Y-axis. The receiving and the transmitting antenna alignment during these tests are depicted in Figure 10. Figure 19 below shows the resulting vertically polarized free-space radiation patterns at that alignment, with the angle Φ as noted in Figure 19 below for the antennas. The patterns remain consistent with the performance of the prior experiments, with radiation focused in the desired half-space (away from the satellite) for both antennas. The satellite body therefore does not adversely affect antenna performance.

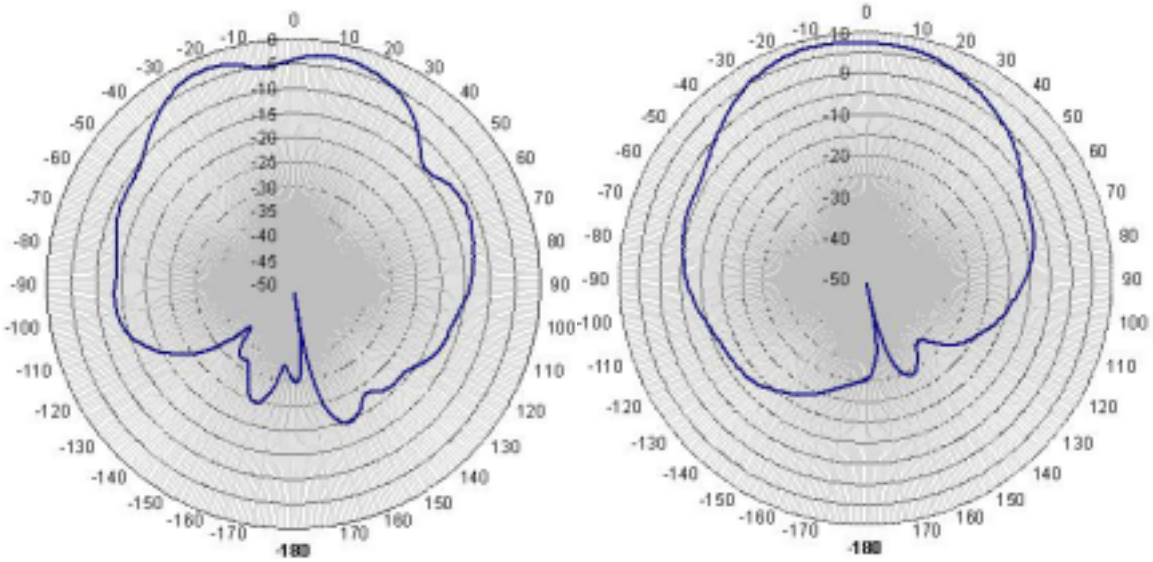

Figure 19. The VPOL Free-space Radiation Patterns of the Receiving Antenna ($\Phi = 90^{\circ}$) and the Transmitting Antenna ($\Phi = -90^{\circ}$) on NPSAT-1

(2) The Antennas Aligned Along the X-Axis. The receiving and the transmitting antenna alignment used during these tests are illustrated in Figure 12. Figure 20 below shows the resulting vertically polarized free-space radiation patterns at that alignment, with the angle Φ as noted in Figure 20 for the two antennas. The patterns remain consistent with the performance of the prior experiments, with radiation focused in the desired half-space (away from the satellite) for both antennas.

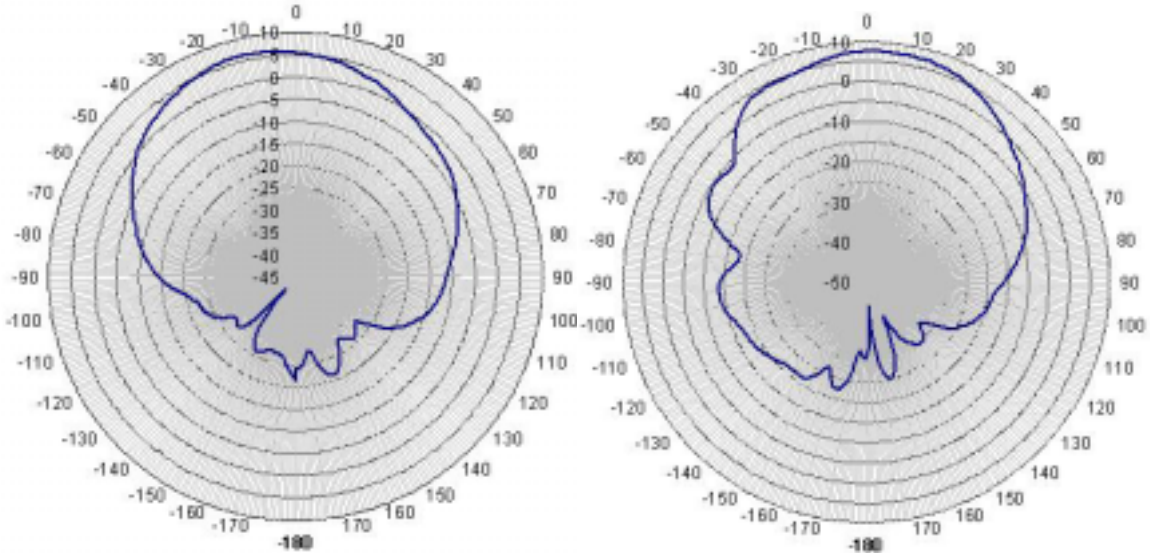

Figure 20. The VPOL Free-space Radiation Patterns of the Receiving Antenna ($\Phi = 0^{\circ}$) and the Transmitting Antenna ($\Phi = 180^{\circ}$) on NPSAT-1

(3) The Antennas Aligned with a Left 45˚ Offset. The receiving and the transmitting antenna alignments during these tests are illustrated in Figure 14. Figure 21 below shows the resulting vertically polarized free-space radiation patterns at that alignment, with the angle Φ as noted in Figure 21 for the two antennas. The patterns remain consistent with the the prior experiments, with radiation focused in the desired half-space (away from the satellite) for both antennas.

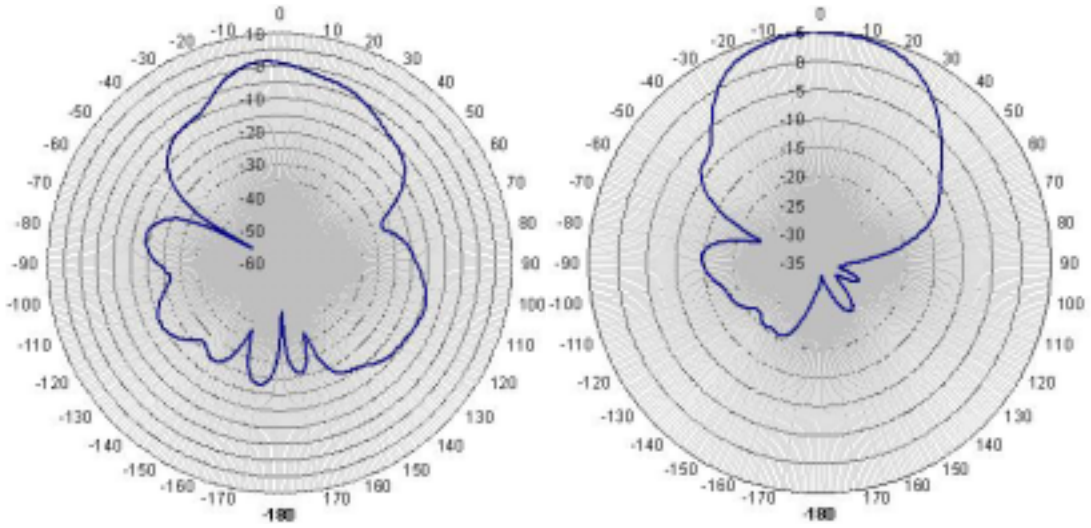

Figure 21. The VPOL Free-space Radiation Patterns of the Receiving Antenna ($\Phi = 135^{\circ}$) and the Transmitting Antenna ($\Phi = -45^{\circ}$) on NPSAT-1

b. Test Results for the Receiving and Transmitting Antennas on NPSAT-1 with the Horn Antenna Horizontally Polarized (HPOL)

(1) The Antennas Aligned Along the Y-Axis. The receiving and the transmitting antenna alignments during these tests are depicted in Figure 10. Figure 22 below shows the resulting horizontally polarized free-space radiation patterns at that alignment, with the angle Φ as noted in Figure 22 for the two antennas. The patterns remain consistent with the performance of the prior experiments, where polarization and alignment were varied, with radiation focused in the desired half-space (away from the satellite) for both antennas.

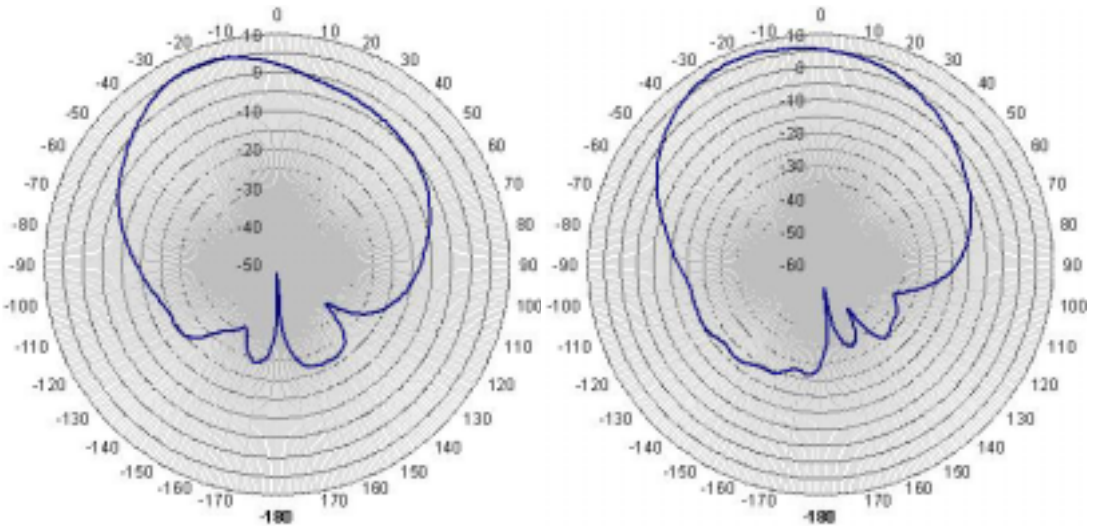

Figure 22. The HPOL Free-space Radiation Patterns of the Receiving Antenna ($\Phi = 90^{\circ}$) and the Transmitting Antenna ($\Phi = -90^{\circ}$) on NPSAT-1

(2) The Antennas Aligned Along the X-Axis. The receiving and the transmitting antenna alignment during these tests are illustrated in Figure 12. Figure 23 shows the resulting horizontally polarized free-space radiation patterns at that alignment, with the angle Φ as noted in Figure 23 for the two antennas. The patterns remain consistent with the performance of the prior experiment, with radiation focused in the desired half-space (away from the satellite) for both antennas.

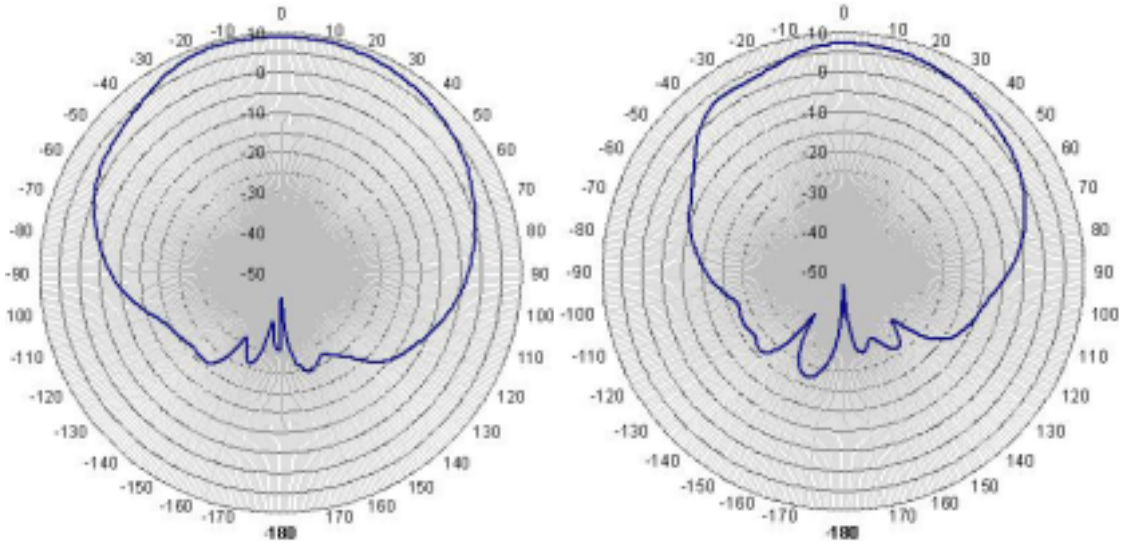

Figure 23. The HPOL Free-space Radiation Patterns of the Receiving Antenna ($\Phi = 0^{\circ}$) and the Transmitting Antenna ($\Phi = 180^{\circ}$) on NPSAT-1

(3) The Antennas Aligned with a Left 45˚ Offset. The receiving and the transmitting antenna alignment during these tests are illustrated in Figure 14. Figure 24 shows the resulting horizontally polarized free-space radiation patterns at that alignment, with the angle Φ as noted in Figure 24 below for the two antennas. The patterns remain consistent with the performance of the prior experiments, with radiation focused in the desired half-space (away from the satellite) for both antennas.

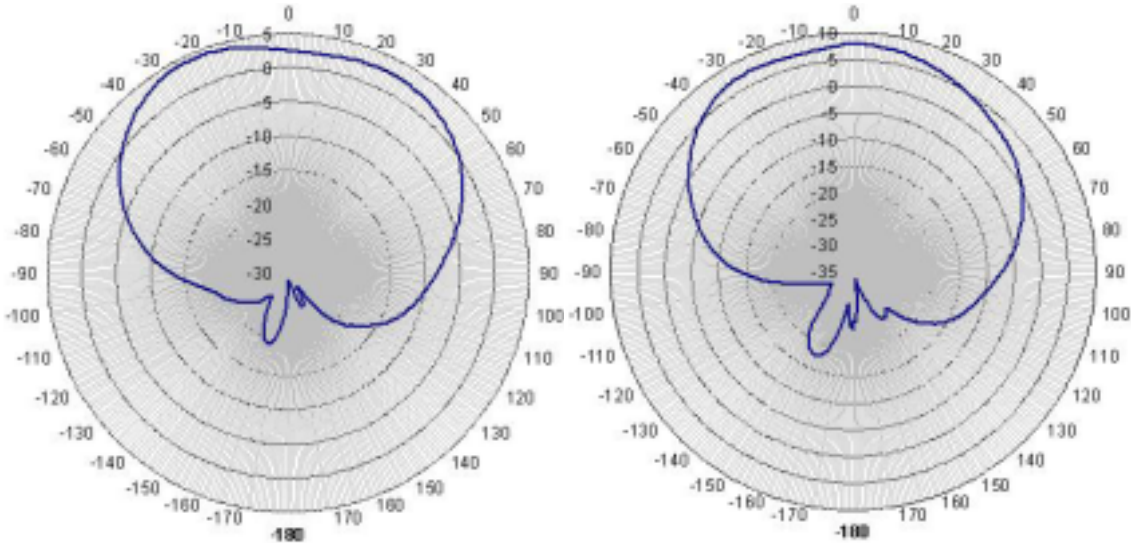

Figure 24. The HPOL Free-space Radiation Patterns of the Receiving Antenna ($\Phi = 135^{\circ}$) and the Transmitting Antenna ($\Phi = -45^{\circ}$) on NPSAT-1

C. ANALYSIS AND SUMMARY

In this Chapter, the test results of the prototype antennas' SWRs, free-space radiation patterns and their associated power gains have been presented. Tests were performed in three phases.

First, the anechoic chamber was prepared and calibrated. Second, the antenna prototypes were tested without using the satellite body model. Results show that both the transmitting and the receiving antennas have 0-dB beamwidth (angular aperture) from 62˚ to 144˚ degrees, depending on the plane (azimuth cut) of the measurement. In addition, the maximum 3-dB beamwidth measured for the transmitting antenna was 107˚ (with the antennas in the 45˚ offset position), while for the receiving antenna the maximum beam-width was 116˚ (when the antenna was oriented horizontally). Mean values for the 0-dB and the 3-dB beamwidths for the receiving antenna, including two different polarizations, were 93.5˚ and 65.5˚, respectively. For the transmitting antenna, these values were 92.8˚ and 70.3˚. Standard deviations for the 0-dB beamwidth of the receiving and the transmitting antennas were 31.6˚ and 21.8˚, respectively. For the 3-dB beamwidth, these values were 31.7˚ and 27.3˚. Table 3 shows the 0-dB and 3-dB beamwidths for both antennas. Comparison of these results with the FDTD software results is detailed in Chapter IV.

	Receiving Antenna Beamwidth				Transmitting Antenna Beamwidth			
PHI	Horn Antenna VPOL		Horn Antenna HPOL		Horn Antenna VPOL		Horn Antenna HPOL	
	0dB	3dB	0dB	3dB	0dB	3dB	0dB	3dB
0	83	57	62	29				
45	72	47	120	90				
90	80	54	144	116				
180					101	82	74	50
225					74	54	119	107
270					73	37	116	92

Table 3. 0-dB and 3-dB Beamwidth for the Transmitting and the Receiving Antennas

The antennas were installed on the NPSAT-1 body model for the final testing phase. The main effect of the body model was observed in the main lobe and the side-lobe gain levels. As shown in Figures 19 through 24, the main lobes of the antennas were widened and flattened, due to the electromagnetic reflection from the surface of the

satellite's body. This resulted in at least a 2 to 3 dB reduction in the maximum gain level. Similarly, the mean and standard deviation values for the 0-dB beamwidth decreased by 2.5% and 10.9%, respectively. For the 3-dB beamwidth, these values also decreased by 1.65% and 41.4% respectively. In summary, the body model of the NPSAT-1 increased the antenna beamwidths, which is actually desirable for providing more uniform coverage regardless of the satellite orientation. Since any increase in beamwidth must come at the expense of reducing the maximum gain, there is a corresponding maximum gain decrease of approximately 3 dB.

This chapter has presented the testing methodology and results of tests for the two antenna prototypes (receiving and transmitting). The antennas were initially tested, as designed, without the inclusion of the NPSAT-1 satellite body. They were re-tested with the portion of the satellite that can influence the characteristics of the antennas, as designed, showing the effects of the satellite body on the performance of the antennas.

IV. COMPARISON OF MEASURED AND COMPUTED RADIATION PATTERNS

In this chapter, test results of the antenna radiation patterns without the satellite body included are compared with the FDTD software results from the initial antenna design as described in Ref. 1.

The comparisons of antenna patterns are performed by presenting the measured data and the calculated data on the same graphs. The chamber used in this research was designed for higher frequencies than those of the NPSAT-1 system. As a result, the absorber material used in the chamber cannot reduce HPOL multipath adequately for these NPSAT-1 antennas. Therefore, only the measurements for the VPOL of the illuminating horn antenna were used in the comparison. The magnitudes of the total gain and the left-hand circular polarization (LHCP) gain, predicted by FDTD, were compared to measured data. Since measurements were performed for linear polarization only, the measured maximum gain would be about 3 dB lower than the simulation results for the LHCP. The comparisons of the transmitting antenna results and the receiving antenna results were separated for readability.

A. COMPARISONS OF TRANSMITTING ANTENNA PATTERNS

1. Comparison for $\Phi = -90^{\circ}$

Comparison of the transmitting antenna prototype measurements with the FDTD software results is depicted in Figure 25. The measured antenna gain is consistent with the calculated absolute gain and calculated LHCP gain. Figure 25 indicates that the transmitting antenna prototype was consistent with the performance predicted by the FDTD software for vertical polarization, with alignment at $\Phi = -90^{\circ}$.

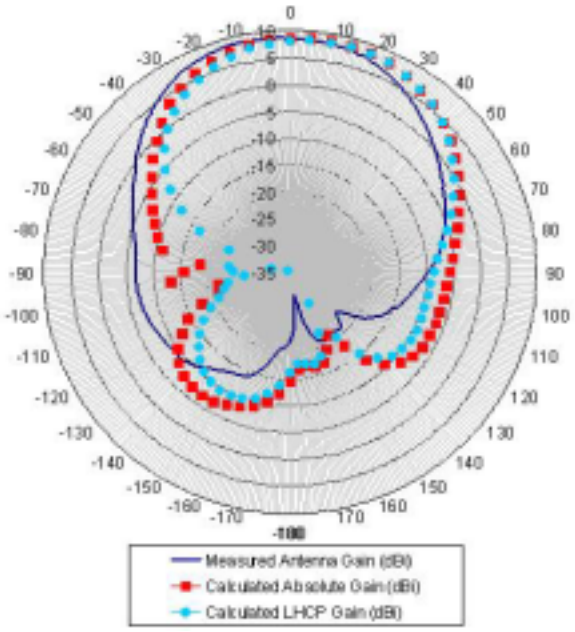

Figure 25. VPOL Measured and Calculated Transmitting Antenna Gain for $\Phi = -90^{\circ}$

2. Comparison for $\Phi = -45^{\circ}$

Figure 26 illustrates the comparison of the transmitting antenna measurements with FDTD software results. The measured antenna gain is consistent with the calculated absolute gain and calculated LHCP gain. Figure 26 indicates that the transmitting antenna prototype was consistent with the performance predicted by the FDTD software for vertical polarization, with alignment at $\Phi = -45^{\circ}$.

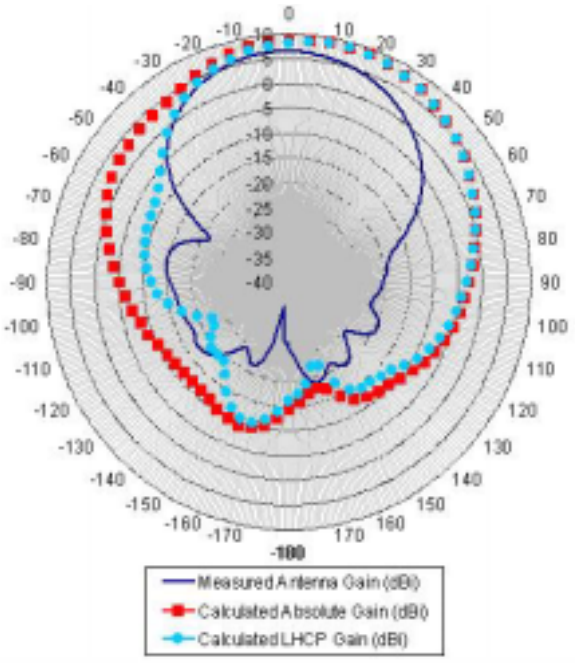

Figure 26. VPOL Measured and Calculated Transmitting Antenna Gain for $\Phi = -45^{\circ}$

3. Comparison for $\Phi = 180^{\circ}$

Comparison of the transmitting antenna prototype measurements with FDTD software results is depicted in Figure 27. The measured antenna gain is consistent with the calculated absolute gain and calculated LHCP gain. Figure 27 indicates that the transmitting antenna prototype was consistent with the performance predicted by the FDTD software for vertical polarization, with alignment at $\Phi = 180^{\circ}$.

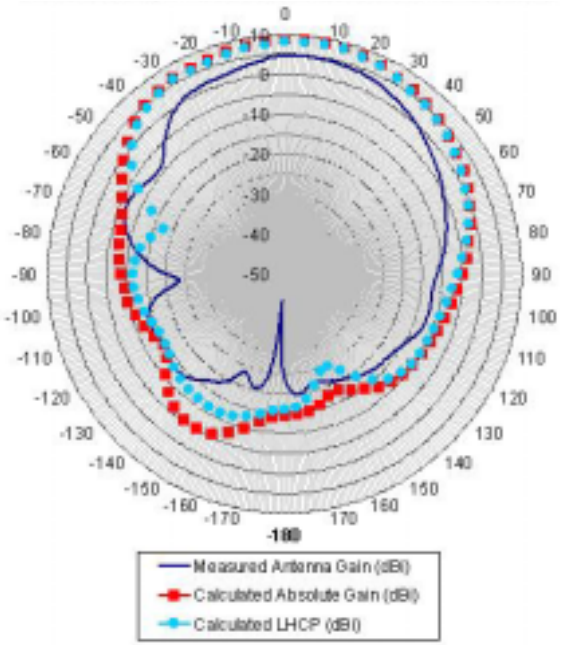

Figure 27. VPOL Measured and Calculated Transmitting Antenna Gain for $\Phi = 180^{\circ}$

B. COMPARISONS OF RECEIVING ANTENNA PATTERNS

1. Comparison for $\Phi = 90^{\circ}$

Figure 28 illustrates the comparison of receiving antenna measurements with FDTD software results. The measured antenna gain is consistent with the calculated absolute gain and calculated LHCP gain. Figure 28 indicates that the receiving antenna prototype was consistent with the performance predicted by the FDTD software for vertical polarization, with alignment at $\Phi = 90^{\circ}$.

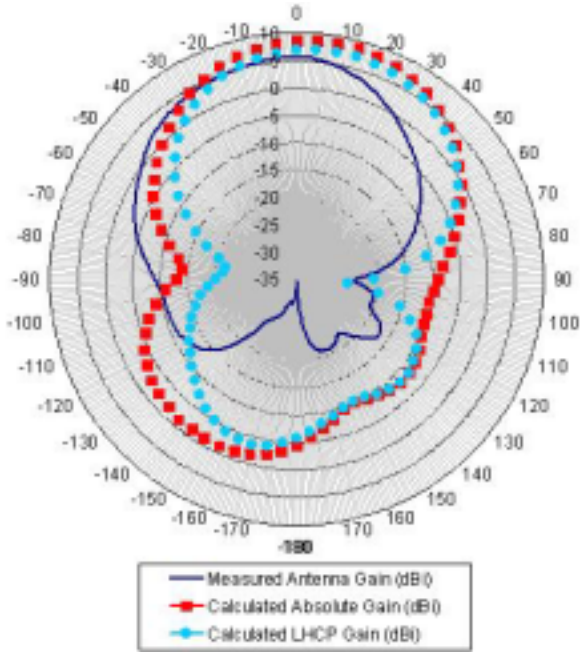

Figure 28. VPOL Measured and Calculated Receiving Antenna Gain for $\Phi = 90^{\circ}$

2. Comparison for $\Phi = 135^{\circ}$

Comparison of the receiving antenna measurements with the FDTD software results is depicted in Figure 29. The measured antenna gain is consistent with the calculated absolute gain and calculated LHCP gain. Figure 29 indicates that the prototype was consistent with the performance predicted by the FDTD software for vertical polarization, with alignment at $\Phi = 135^{\circ}$.

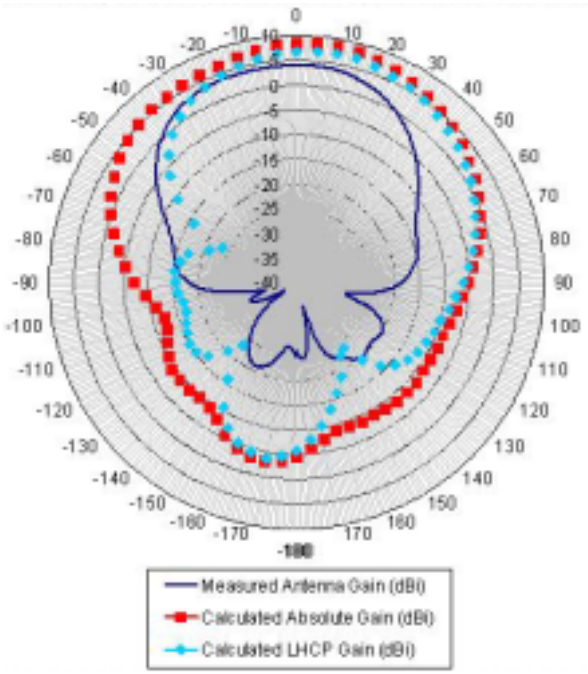

Figure 29. VPOL Measured and Calculated Receiving Antenna Gain for $\Phi = 135^{\circ}$

3. Comparison for $\Phi = 0^{\circ}$

Figure 30 illustrates the comparison of the receiving antenna measurements with the FDTD software results. The measured antenna gain is consistent with the calculated absolute gain and calculated LHCP gain. Figure 30 indicates that the prototype was consistent with the performance predicted by the FDTD software for vertical polarization, with alignment at $\Phi = 0^{\circ}$.

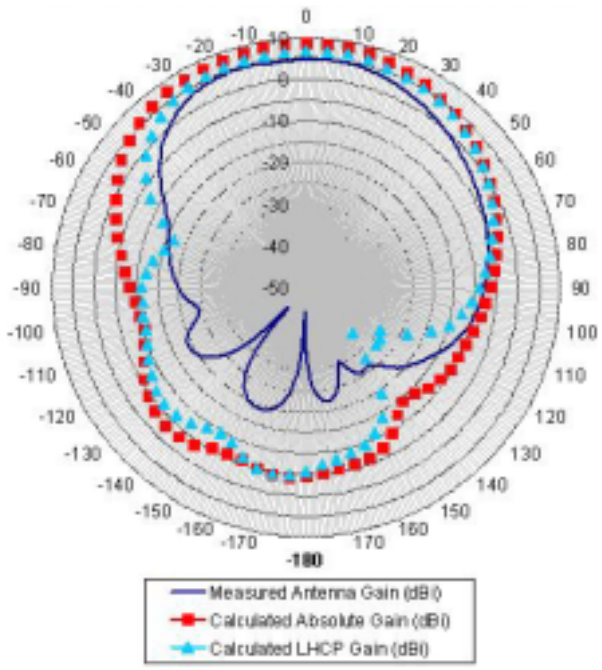

Figure 30. VPOL Measured and Calculated Receiving Antenna Gain for $\Phi = 0^{\circ}$

C. SWR COMPARISON

In his thesis, LTJG Mahmut Erel detailed the process of meeting the VSWR requirement of the NPSAT-1. Figures 31 and 32 illustrate the predicted values for the VSWR.

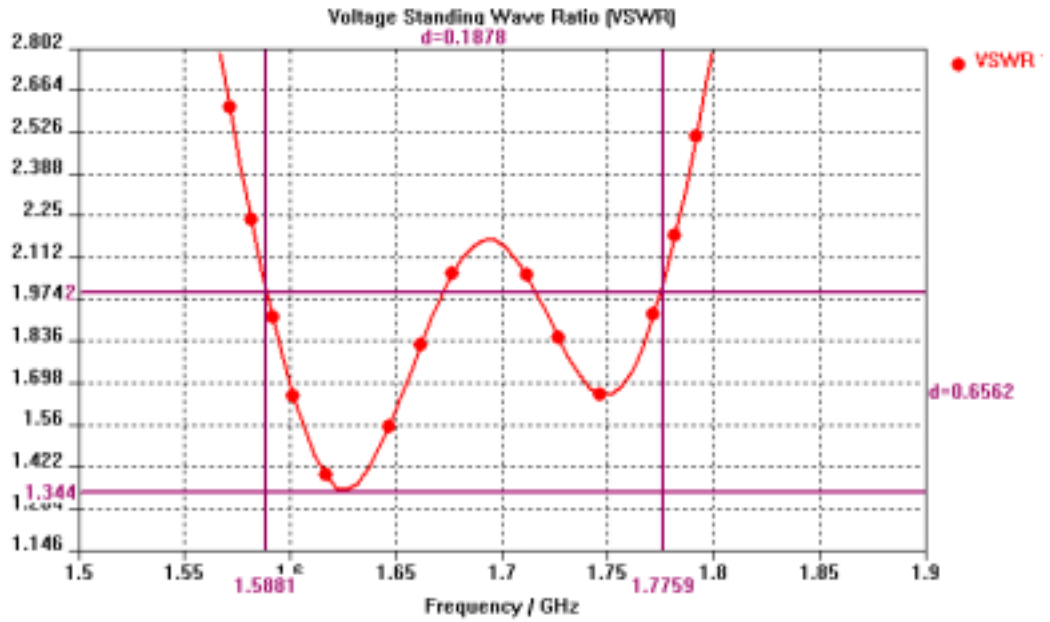

Figure 31. Calculated VSWR vs. Frequency for the Receiving Antenna [From Ref.1]

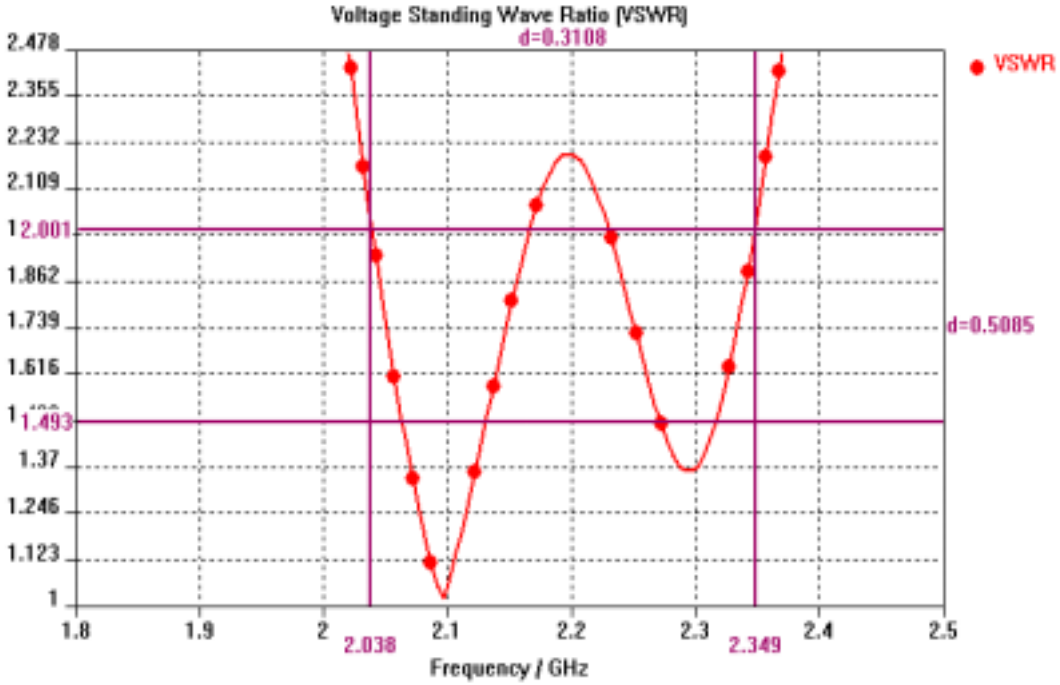

Figure 32. Calculated VSWR vs. Frequency for the Transmitting Antenna [From Ref.1]

Erel cites a VSWR of 2 for the transmitting antenna and 1.86 for the receiving antenna, at their designated center frequencies. The measured VSWR values for the

prototype antennas, discussed in Chapter III, are 1.89 for the transmitting antenna and 1.77 for the receiving antenna. Hence, 5.56% improvement in the transmitting antenna VSWR and 4.98% improvement in the receiving antenna VSWR were observed.

D. ANALYSIS AND SUMMARY

In this section, the free-space radiation patterns and their associated gain levels, as well as the SWR results for the transmitting and the receiving antenna, are compared and examined.

The anechoic chamber at NPS is specifically designed for experiments in the I-band and J-band (8-18 GHz). The radiation for operating frequencies of NPSAT-1 antennas are too low to be completely absorbed by the absorbing material covering the chamber walls. Some multipath effects were observed, especially when the illuminating horn antenna is horizontally polarized. The multipath is formed by multiple electromagnetic waves arriving at the receiving antenna from directions other than line-of-sight (LOS). Due to this multipath, the electromagnetic field at the receiving antenna becomes a vector sum of the LOS signal and its phase-delayed and amplitude-scaled reflections. In this particular anechoic chamber at the operating frequency range of interest, the horizontally polarized signals generate more multipath than the vertically polarized signals. Equation 4-1 shows how the field at the receiving antenna differs from the free-space propagation values.

$$F = \left| 1 + \rho e^{j\Phi - jk_0(R_2 - R_1)} \right| , \tag{4.1}$$

where the factor F is the *path-gain factor*, $\rho e^{j\Phi}$ is the reflection coefficient, also known as Γ, k_0 is the wave number equal to $2\pi/\lambda$, and R_2 and R_1 are the path lengths of the reflected ray and the direct (LOS) ray respectively. In the formula above, the only unknown for the anechoic chamber is the reflection coefficient, $\rho e^{j\Phi}$. The reflection coefficients for vertical and horizontal polarization are given by

$$\rho e^{j\phi} = \frac{(\kappa - j\chi)\sin\psi - \sqrt{(\kappa - j\chi) - \cos^2\psi}}{(\kappa - j\chi)\sin\psi + \sqrt{(\kappa - j\chi) - \cos^2\psi}} , \qquad \text{vertical polarization} \tag{4.2}$$

$$\rho e^{j\phi} = \frac{\sin\psi - \sqrt{(\kappa - j\chi) - \cos^2\psi}}{\sin\psi + \sqrt{(\kappa - j\chi) - \cos^2\psi}} \quad , \qquad \text{horizontal polarization} \qquad (4.3)$$

where $\chi = \sigma/\omega\varepsilon_0$, and the angle that the reflected ray forms with the normal to the reflecting surface is denoted ψ. For typical outdoor environments, the conductivity σ may range from 10^{-3} to $3\cdot10^{-3}$ Seimens while typical values for dielectric constant κ are around 15 [3]. Note that the respective values for the anechoic chamber are not known precisely and are frequency dependent.

In many cases, the *path gain factor*, *F*, is between 2 dB and 4 dB. Initial evaluation of the data shows that the measured data diverged an average of +1.7 dB from the calculated data. However, measurements are based on linear (vertical and horizontal) polarization, while software predictions were made for circular polarization. Therefore the measured data should show peak gains (for linear polarization) about 3 dB lower than peak gains for circular polarization. Under perfect test conditions, the measured data would not exceed values calculated by software. Differences observed are explained by the multipath effect outlined above. Since differences are far more prominent for horizontal polarization than for vertical polarization, values measured for horizontal polarization have not been included in the comparison. Similarly, only the calculated total field magnitude and the LHCP field magnitude values were included, since LHCP is the preferred circular polarization type for NPSAT-1.

The receiving antenna measurements show a mean value of 78.3˚ for the 0-dB beamwidth while the predicted mean value is 99.3˚. In addition, the measured 3-dB beamwidth was 52.6˚ but was 78˚ for calculated data. The average value of the measured 0-dB beamwidth was 21.1% lower than the predicted value, and the measured 3-dB beamwidth was 32.4% lower than the predicted value. Furthermore, the mean value for maximum measured gain was 4.72 dB, while the predicted value was 6.93 dB. This shows a 31.8% (2.21 dB) difference between measured and predicted values. Note that the theoretical difference for pure LHCP and linear polarization measurements without multipath should have been exactly 3 dB. Therefore, peak gain measurements are remarkably close (less than 1-dB difference) to predicted values. The beamwidth differences are also a consequence of the measurements using linear polarization rather than

circular polarization. Note that beamwidth measurements produced percentage differences comparable to differences in measured and predicted peak gain, which are due to the linear (measured) versus circular (predicted) polarization. However, since the ground stations will use linear polarization, the measured results for linear polarization are representative of the performance that can be expected from these antennas in actual use on NPSAT-1.

For the transmitting antenna, mean values of the 0-dB beamwidth measured and predicted data were 82.6˚ and 108.3˚, respectively. The difference is 23.7%. For the 3-dB beamwidth, the values are 57.6˚ and 88˚, respectively, and the difference is 34.4%. In addition, mean values for maximum gain were 6.63 dB for measured data and 8.42 dB for calculated data, with a difference of 21.2% (1.79 dB).

Table 4 shows the result for the measured and the estimated data.

	Receiving Antenna						Tranmitting Antenna					
	Measured			Estimated			Measured			Estimated		
PHI	0dB	3dB	Max Gain	0dB	3dB	Max Gain	0dB	3dB	Max Gain	0dB	3dB	Max Gain
0	83	57	5.56	93	73	7.01						
45	72	47	3.96	100	75	6.99						
90	80	54	4.66	105	86	6.80						
180							101	82	8.78	98	80	8.42
225							74	54	6.44	110	88	8.63
270							73	37	4.68	117	96	8.24

Table 4. 0-dB and 3-dB Beamwidths (in degrees) and Maximum Gain Levels (in dBi) for Transmitting and Receiving Antennas

THIS PAGE INTENTIONALLY LEFT BLANK

V. CONCLUSIONS AND RECOMMENDATIONS

A. CONCLUSIONS

The measurements and FDTD software models validated the NPSAT-1 antenna system design. The antenna system design satisfies the NPSAT-1 requirements for impedance bandwidth, low profile, and broad radiation patterns. The design also satisfies the pre-launch specification of fitting into the EPAS canister. The measured SWR was 1.89 for the transmitting antenna and 1.77 for the receiving antenna. These values are also within the NPSAT-1 SWR requirement of maximum SWR of 2:1. The feed system for the antennas consists of two simple SMA connectors soldered to the patches, mounted on the ground plane. Hence, the necessary RF power connection to the antennas can be easily achieved.

The prototype antenna radiation patterns were validated by the comparison of anechoic chamber pattern measurements with those generated by the FTDT software.

B. RECOMMENDATIONS

All measurements were performed on prototype antennas. These antennas have some small differences from the original design as discussed in Chapter II. The prototype antennas were not tested against vibration and shock, electromagnetic compatibility (EMC), or thermal environment specifications. Furthermore, the antenna system should be tested with the final space-flight-ready NPSAT-1, to compare its final radiation patterns and power gains to those presented in this thesis. Tests similar to those detailed in this thesis can be performed when measuring the coupling between the antennas, although such measurements may be difficult, as the predicted coupling is very low (below –30 dB). In addition to the tests mentioned above, a top-to-bottom mutual coupling test can be performed to analyze the effects of the two separate antenna systems, which will be installed on the top and the bottom of the satellite.

THIS PAGE INTENTIONALLY LEFT BLANK

LIST OF REFERENCES

1. Erel, M., *Design of a Microstrip Patch Antenna for the NPSAT-1*, Master's Thesis, Naval Postgraduate School, Monterey, CA, December 2002.
2. Rappaport, T.S., *Wireless Communications, Principles and Practice* 2nd ed., Prentice Hall, Upper Saddle River, NJ, 2002.
3. Hirasawa, K., Haneishi, M., *Analysis, Design, and Measurement of Small and Low-Profile Antennas*, Artech House, Inc., Norwood, MA, 1992.
4. **www.whatis.com** 12/1/2002

THIS PAGE INTENTIONALLY LEFT BLANK

BIBLIOGRAPHY

Bahl, I.J. and Bhartia, P., *Microstrip Antennas*, Artech House Inc., Dedham, MA, 1980.

Balanis, C.A., *Antenna Theory and Design*, 2nd ed., John Wiley and Sons Inc., NY, 1997.

Booton, R. C., Jr. *Computational Methods for Electromagnetics and Microwaves. Finite Difference Time Domain Method.* Chapter 4, pp 59-73., John Wiley and Sons Inc., NY, 1992.

Garg, R., Bhartia, P., Bahl, I., Ittipiboon, A., *Microstrip Antenna Design Handbook,* Artech House, Inc, Norwood, MA, 2001.

Lee, K.F. and Chen, W., *Advances in Microstrip and Printed Antennas,* John Wiley and Sons Inc., NY, 1997.

Pozar, D.M., *Microwave Engineering*, 2nd ed., John Wiley and Sons, Inc.,NY, 1998.

Pozar, D.M. and Schaubert, D., *Microstrip Antennas-The Analysis and Design of Microstrip Antennas and Arrays,* IEEE Press, Piscataway, NJ, 1995.

Stutzman W.L. and Thiele G.A., *Antenna Theory and Design*, John Wiley and Sons Inc., NY, 1981.

Ulaby, F., *Fundamentals of Applied Electromagnetics*, Prentice Hall, Upper Saddle River, NJ, 1996.

THIS PAGE INTENTIONALLY LEFT BLANK

INITIAL DISTRIBUTION LIST

1. Defense Technical Information Center
   Ft. Belvoir, VA

2. Dudley Knox Library
   Naval Postgraduate School
   Monterey, CA

3. Chairman, Department of Electrical and Computer Engineering
   Naval Postgraduate School
   Monterey, CA

4. Prof. Jovan Lebaric
   Naval Postgraduate School
   Monterey, CA

5. Prof. Richard W. Adler
   Naval Postgraduate School
   Monterey, CA

6. Deniz Kuvvetleri Komutanlığı
   Ankara, TK

7. Deniz Harp Okulu Kütüphanesi
   İstanbul, TK

8. LTJG. İlhan Gökben
   İstanbul, TK

9. David Rigmaiden
   Naval Postgraduate School
   Monterey, CA